PASJ: Publ. Astron. Soc. Japan **63**, 1117–1138, 2011 October 25

Asteroid Catalog Using AKARI: AKARI/IRC Mid-Infrared Asteroid Survey

Fumihiko USUI,[1] Daisuke KURODA,[2] Thomas G. MÜLLER,[3] Sunao HASEGAWA,[1] Masateru ISHIGURO,[4] Takafumi OOTSUBO,[5] Daisuke ISHIHARA,[6] Hirokazu KATAZA,[1] Satoshi TAKITA,[1] Shinki OYABU,[6] Munetaka UENO,[1] Hideo MATSUHARA,[1] and Takashi ONAKA[7]

[1]*Institute of Space and Astronautical Science, Japan Aerospace Exploration Agency, 3-1-1 Yoshinodai, Chuo-ku, Sagamihara 252-5210*
usui@ir.isas.jaxa.jp

[2]*Okayama Astrophysical Observatory, National Astronomical Observatory, 3037-5 Honjo, Kamogata-cho, Asakuchi, Okayama 719-0232*

[3]*Max-Planck-Institut für Extraterrestrische Physik, Giessenbachstraße, 85748 Garching, Germany*

[4]*Department of Physics and Astronomy, Seoul National University, San 56-1, Shillim-dong Gwanak-gu, Seoul 151-742, South Korea*

[5]*Astronomical Institute, Tohoku University, 6-3 Aoba, Aramaki, Aoba-ku, Sendai 980-8578*

[6]*Graduate School of Science, Nagoya University, Furo-cho, Chikusa-ku, Nagoya 464-8601*

[7]*Department of Astronomy, Graduate School of Science, The University of Tokyo, 7-3-1 Hongo, Bunkyo-ku, Tokyo 113-0033*

(Received 2011 February 10; accepted 2011 June 3)

Abstract

We present the results of an unbiased asteroid survey in the mid-infrared wavelength region with the Infrared Camera (IRC) on board the Japanese infrared satellite AKARI. About 20% of the point source events recorded in the AKARI All-Sky Survey observations are not used for the IRC Point Source Catalog (IRC-PSC) in its production process because of a lack of multiple detection by position. Asteroids, which are moving objects on the celestial sphere, remain in these "residual events". We identify asteroids out of the residual events by matching them with the positions of known asteroids. For the identified asteroids, we calculate the size and albedo based on the Standard Thermal Model. Finally we have a new brand of asteroid catalog, named the Asteroid Catalog Using AKARI (AcuA), which contains 5120 objects, about twice as many as the IRAS asteroid catalog. The catalog objects comprise 4953 main belt asteroids, 58 near-Earth asteroids, and 109 Jovian Trojan asteroids. The catalog is publicly available via the Internet.

Key words: catalogs — infrared: solar system — minor planets, asteroids — space vehicles: instruments — surveys

1. Introduction

The physical properties of asteroids are fundamental to understanding the formation process of our planetary system. In the present solar system, asteroids are thought to be the primary remnants of the original building blocks that formed the planets. They contain a record of the initial conditions of our solar nebula of 4.6 Gyr ago. The composition and size distribution of asteroids in the asteroid belt provide significant information on their evolution history, although they have experienced mutual collisions, mass depletion, mixing, and thermal differentiation, which have shaped their present-day physical and orbital properties.

The size and albedo are the basic physical properties of the asteroid. In some cases, by combining the size and the mass, which are precisely measured using modern techniques (Hilton 2002), the bulk density of the asteroid can be estimated (Britt et al. 2002). It is a powerful indicator to investigate the macroscopic porosity and the inner structure of an asteroid. The total mass and the size distribution of asteroids are crucial to understanding the history of the solar system (Bottke et al. 2005). The mineralogy and elemental composition of asteroids can also be estimated from the albedo (Burbine et al. 2008).

There are several survey catalogs of asteroids: the 2MASS Asteroid Catalog (Sykes et al. 2000) compiles near-infrared colors of 1054 asteroids based on the Two Micron All Sky Survey; the Subaru Main Belt Asteroid Survey (SMBAS: Yoshida & Nakamura 2007) gives the size and color distributions of 1838 asteroids observed with the Subaru telescope; the SDSS Moving Object Catalog (SDSS MOC: Parker et al. 2008) consists of multicolor photometry of $\sim$88000 asteroids from the Sloan Digital Sky Survey; the Sub-Kilometer Asteroid Diameter Survey (SKAD: Gladman et al. 2009) provides the size distribution of 1087 asteroids based on observations with the 4 m Mayall telescope at Kitt Peak National Observatory. While these catalogs are based on optical to near-infrared observations, the size and albedo of asteroids are decoupled, and can be determined solely independently, once mid-infrared observations are accomplished (Lebofsky & Spencer 1989; Bowell et al. 1989; Harris & Lagerros 2002).

A radiometric technique was first applied to determine the size and albedo of asteroids with ground-based observatories by Allen (1970) for 4 Vesta, by Allen (1971) for 1 Ceres, 3 Juno, and 4 Vesta, and by Matson (1971) for 26 major main-belt asteroids. A pioneering systematic asteroid survey with a space-borne telescope was made by the Infrared Astronomical Satellite (IRAS) launched in 1983 (Neugebauer et al. 1984). IRAS observed more than 96% of the sky at the mid- and far-infrared 4 bands (12, 25, 60, and 100 μm) during the 10-month mission life. It derived the size and

albedo of $\sim$2200 asteroids (Tedesco et al. 2002a).[1] Another serendipitous survey was carried out by the Midcourse Space Experiment (MSX) launched in 1996 (Mill et al. 1994; Price et al. 2001). It observed $\sim$10% of the sky at 6 bands of 4.29, 4.35, 8.28, 12.13, 14.65, and 21.34 μm; $\sim$160 asteroids were identified, for which the size and albedo were provided (Tedesco et al. 2002b).[2] Also, the Infrared Space Observatory (ISO) launched in 1995 (Kessler et al. 1996) made yet-another part-of-sky survey, and observed several planets, satellites, comets, and asteroids at infrared wavelengths (Müller et al. 2002). Despite these extensive past surveys, the asteroids for which the size and albedo have been determined are still only 0.5% of those with known orbital elements.

AKARI is the first Japanese space mission dedicated to infrared astronomy (Murakami et al. 2007). AKARI is equipped with a 68.5 cm cooled telescope, a 170-liter container of superfluid liquid Helium (LHe), and two sets of two-stage Stirling cycle coolers. The focal plane instruments consist of the Infrared Camera (IRC) (Onaka et al. 2007) and the Far-Infrared Surveyor (FIS) (Kawada et al. 2007), that cover the spectral ranges of 2–26 μm and 50–180 μm, respectively. AKARI carried out the second generation infrared all-sky survey after IRAS. The All-Sky Survey is one of the main objectives of the AKARI mission in addition to pointed observations. It surveyed the whole sky at 6 bands in the mid- to far-infrared spectral range with a solar elongation of $90^\circ \pm 1^\circ$ so as to avoid radiation from Earth and the Sun. The AKARI satellite was launched on 2006 February 21 (UT). The All-Sky Survey had continued until the LHe was boiled off on 2007 August 26. In total, more than 96% of the sky had been observed more than twice[3] during the cryogenic mission phase.

In this paper, we present a catalog of the size and geometric albedo of asteroids based on the IRC All-Sky Survey data. The IRC All-Sky Survey was carried out at two bands in the mid-infrared: *S9W* (6.7–11.6 μm) and *L18W* (13.9–25.6 μm). The IRC All-Sky Survey has advantages over the IRAS survey in detecting asteroids in the sensitivity and spatial resolution, both of which have been improved by an order of magnitude. The 5 σ detection limits at the *S9W* and *L18W* bands are 50 and 90 mJy, respectively, and the spatial resolution of the IRC in the All-Sky Survey mode was $\sim 10''$ per pixel (Ishihara et al. 2010). Point-source detection events were extracted and processed in the IRC All-Sky Survey observation data, from which the IRC Point Source Catalog (IRC-PSC: Ishihara et al. 2010) was produced after checking the positions of sources with multiple detection. About 20% of the extracted events in the All-Sky Survey data are not used for the IRC-PSC, because of a lack of confirmation detection. We identify asteroids out of the events excluded from the IRC-PSC. In this process, we search for events whose positions agree with those of asteroids with known orbits. The asteroid positions were calculated by numerical integration of the orbit. We have not made any attempt to discover new asteroids in this project, whose orbital elements are not archived in the database. For each identified object, we calculated the size and albedo using the Standard Thermal Model of asteroids (Lebofsky et al. 1986). Finally, we obtained an unbiased, homogeneous asteroid catalog, which contains 5120 objects in total, twice as many as the IRAS asteroid catalog. This corresponds to $\sim$1% of all the asteroids with known orbital elements.

This paper is organized as follows: In section 2, we describe the data reduction and the creation procedure of the asteroid catalog from the IRC All-Sky Survey data. In section 3, we describe characteristics of the obtained catalog. In section 4, we summarize the paper and discuss future prospects. Scientific output from this catalog will be discussed at length in a forthcoming paper (F. Usui et al. in preparation).

2. Data Processing and Catalog Creation

2.1. The AKARI IRC All-Sky Survey

The AKARI All-Sky Survey observation started on 2006 April 24 as part of performance verifications of the instruments prior to nominal observations, which started on 2006 May 8. In the All-Sky Survey observation mode, AKARI always points the telescope in the direction perpendicular to the Sun–Earth line, and rotates once every orbital revolution in a Sun-synchronous polar orbit (see figure 4 in Murakami et al. 2007). The telescope looks in the direction opposite to the Earth's center to make continuous scans on the sky at a rate of $216'' \, s^{-1}$. The orbital plane rotates around the axis of Earth at the rate of the orbital motion of Earth, and thus the whole sky can be observed in half a year. During the 18-month course of the AKARI LHe mission, a given area of the sky was observed three or more times on average, depending on the ecliptic latitude. A large number of scan observations were made in the ecliptic polar regions, while only two scan observations (overlapping halves of the FOV in contiguous scans) were possible in half a year for given spots on the plane of the ecliptic. In this regard, solar-system objects near the ecliptic give few observation opportunities with AKARI. In addition to the low visibility, other conditions further limit the observation opportunities near the ecliptic, including the disturbances such as the Moon and the South Atlantic Anomaly (SAA), that is a high-density region of charged particles (mainly protons) at an altitude of a few hundred km above Brazil. Another complication arose as to the operation after the first half year, which was called the offset survey. It was an "aggressive" operation to swing the scan path to complement imperfect scan observations in the first half year, which had been made in a "passive" survey mode. The first half-year survey left many regions of the sky unobserved due to the Moon and the SAA, to conflicts with pointed observations, and to telemetry downlink failures. To make up observations of these regions and to increase the completeness of the sky coverage, the scan path was shifted from the nominal direction to fill the gaps on almost every orbit in the second and third halves of years (Y. Doi et al. in preparation). For observations of solar-system objects, the offset survey operation has both positive and negative effects. Some objects may lose observation opportunities completely,

[1] The actual data is avaliable at NASA Planetary Data System, Supplemental IRAS Minor Planet Survey (SIMPS) ⟨http://sbn.psi.edu/pds/asteroid/IRAS_A_FPA_3_RDR_IMPS_V6_0/⟩.

[2] The actual data is avaliable at NASA Planetary Data System, MSX Infrared Minor Planet Survey (MIMPS) ⟨http://sbn.psi.edu/pds/asteroid/MSX_A_SPIRIT3_5_SBN0003_MIMPS_V1_0/⟩.

[3] AKARI/IRC All-Sky Survey Point Source Catalogue Version 1.0 Release Note ⟨http://www.ir.isas.jaxa.jp/AKARI/Observation/PSC/Public/RN/AKARI-IRC_PSC_V1_RN.pdf⟩.

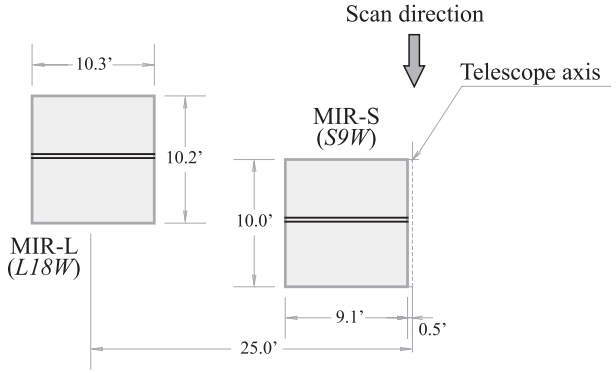

Fig. 1. Schematic view of the focal-plane layout of the IRC *S9W* (MIR-S) and *L18W* (MIR-L) detectors. Details are given in Murakami et al. (2007) and Onaka et al. (2007). The two solid lines in each detector denote the positions of the operating pixel rows (the 117th and 125th of the total 256 rows) for the All-Sky Survey observation mode. The separation between the two rows is exaggerated in figure. Combining these two rows in the data processing, we remove false signals due to cosmic ray hits (millisec confirmation, Ishihara et al. 2010).

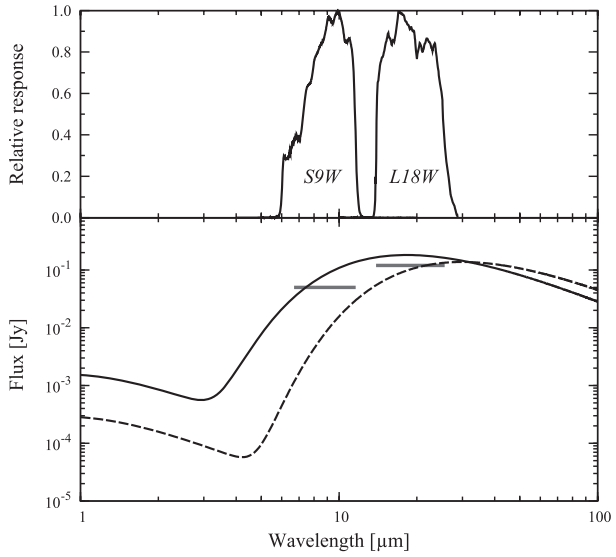

Fig. 2. Upper: Relative spectral response of *S9W* and *L18W* from AKARI web site.[4] Lower: Model spectra of asteroids including the reflected sunlight and the thermal emission are shown for reference. The solid line indicates the model flux of the asteroid with $d = 5$ km, $p_{\rm v} = 0.3$, and $R_{\rm h} = 1.56$ AU, where d, $p_{\rm v}$, and $R_{\rm h}$ are the size in diameter, the geometric albedo, and the heliocentric distance, respectively. The Standard Thermal Model (sub-subsection 2.2.4) is used for the calculation. The dashed line indicates another model flux with $d = 33$ km, $p_{\rm v} = 0.08$, and $R_{\rm h} = 4.6$ AU. Each of the two asteroids represents a lower limit in the size at the corresponding distance in the AKARI survey. The horizontal bars also show the detection limits of *S9W* and *L18W*.

while others may increase the number of detections drastically.

Since solar-system objects have their orbital motions, detection cannot be confirmed in principle by the position on the celestial sphere. Moreover, *S9W* and *L18W* observed different sky regions $\sim 25'$ apart in the cross-scan direction from each other because of the configuration on the focal plane (figure 1), and an object was not observed with the 2 bands in the same scan orbit. Therefore, a single event of a point source needs to be examined without stacking.

Figure 2 shows the normalized spectral response function of *S9W* and *L18W*. The calculated model fluxes of asteroids are also shown.

In the following, we describe how asteroid events are extracted and identified in the All-Sky Survey observation, and how their size and albedo are derived.

2.2. *The Outline of Data Processing*

An outline of data processing to extract asteroid events is summarized in the following (see also figure 3):

1. Point sources are extracted by pipeline processing from the IRC All-Sky Survey image data. The positions of extracted sources are matched with each other, and the sources detected more than twice are regarded as being confirmed ones and cataloged in the IRC-PSC. The detected sources not cataloged in the IRC-PSC are considered to consist of extended sources, signals due to high-energy particles, geostationary satellites, and solar-system objects such as asteroids and comets (sub-subsection 2.2.1). Hereafter, individual extracted point sources in the All-Sky Survey are called "events", and a summary of the events is called an "event list". The physical flux of each event is derived in the pipeline processing.
2. Identification of an event with an asteroid is made based on the predicted position of the asteroid with known orbital elements (sub-subsection 2.2.2).
3. Color corrections are applied to the fluxes of those events identified as asteroids, while taking into account the heliocentric distance of the object. Events with large errors, or those with very small fluxes are struck out from the list at this stage (sub-subsection 2.2.3).
4. The size and albedo of each identified event are calculated based on the Standard Thermal Model (sub-subsection 2.2.4).
5. Further screening of the sources is performed and the final catalog is prepared (sub-subsection 2.2.5).

2.2.1. *Event list for asteroid identification*

The present asteroid catalog is a secondary product of the IRC-PSC. Thus, corrections for detector anomalies, image reconstruction, point-source extraction, pointing reconstruction, and flux calibration are applied in the same manner as in the IRC-PSC processing (Ishihara et al. 2010). About 25% (*S9W*) and 18% (*L18W*) of the total events are not used for the IRC-PSC, and are analyzed in the present process (table 1).

2.2.2. *Asteroid identification*

Identifying events as asteroids is made based on the orbital calculation of the asteroids with known orbital elements. N-body simulations including gravitational perturbations with the Moon, eight planets, Ceres, Pallas, Vesta, and Pluto are employed for the calculation. We regard the other asteroids as massless particles. The orbital elements of the asteroids are taken from the Asteroid Orbital Elements Database

[4] ⟨http://www.ir.isas.jaxa.jp/ASTRO-F/Observation/RSRF/IRC_FAD/⟩.

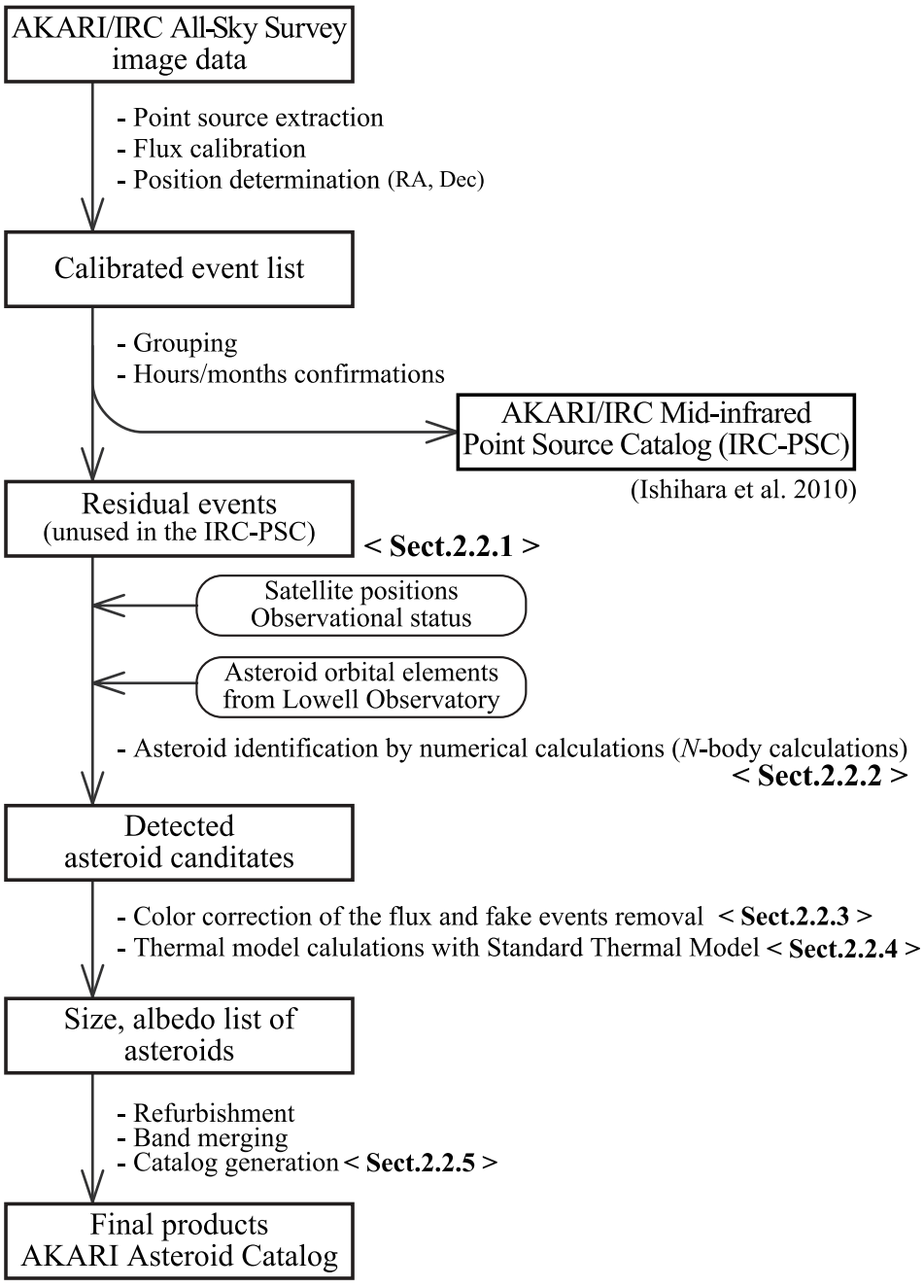

Fig. 3. Outline of data processing to create the asteroid catalog.

(Bowell et al. 1994) distributed at Lowell Observatory[5] at the epoch of 2010 April 14.0. It has 503681 entries, which consist of 233968 numbered and 269713 unnumbered asteroids. Objects with large uncertainties in the orbital parameters, indicated as non-zero integers for the orbit computation in the database, are excluded. They include 19 numbered asteroids and 8759 unnumbered. The positions of the Sun, planets, Moon, and Pluto are taken from DE405 JPL Planetary and Lunar Ephemerides in the J2000.0 equatorial coordinates at the NASA Jet Propulsion Laboratory. A Runge–Kutta–Nystrom 12(10) method (Dormand et al. 1987) is used for the time integration with a variable time step.

The asteroid identification process is performed in the following steps:

1. A two-body (i.e., the Sun and a given asteroid) problem is solved at the epoch of the orbital elements of the asteroid to estimate the velocity and acceleration.
2. Given the observation time of an event detected by AKARI, the position of an asteroid is calculated back to that observation time by an N-body simulation. The integration time step is initially set as 1 d, and varied

[5] The data is available at ⟨ftp://ftp.lowell.edu/pub/elgb/astorb.html⟩.

Table 1. Number of events for each processing step.*

	Event	*S9W*	*L18W*
(a)	All events	4762074	1244249
(b)	Events employed in the IRC-PSC	3882122	936231
(c)	Residual events	879952	308018
(d)	Events identified as asteroids	6924	13760
(e)	Asteroids in the final catalog	2507	5010
(f)	Asteroids detected overall	5120	

* (a) "Event" indicates an individual detection of a point source in the All-Sky Survey data. (b) Events confirmed as a point source by multiple detections at the same celestial position (Ishihara et al. 2010). (c) Unused events in the IRC-PSC: (c) = (a) − (b). (d) Events identified as asteroids by the estimated positions. False identifications are excluded. (e) Asteroids listed in the final catalog. (f) Asteroids detected with either *S9W* or *L18W* or both.

appropriately later in the following calculation. The calculated position is converted to the J2000.0 astrometric coordinates (i.e., the coordinates are revised with the correction for the light-time) since the positions of the events in the All-Sky Survey are given in the J2000.0 coordinates.

AKARI has a Sun-synchronous polar orbit at an altitude of 700 km. The parallax between the geocenter and the spacecraft is not negligible, particularly if an object is one of near-Earth asteroids. The parallax amounts to an order of 30″. Thus, the apparent position relative to the AKARI spacecraft needs to be calculated. The spacecraft position is obtained by interpolation of the data from the AKARI observational scheduling tool, which serves for present purposes with sufficient accuracy.

3. The calculated positions are compared with those of events detected in the All-Sky Survey. If the predicted position of an asteroid is located within 2.′5 of the position of an event, the process goes to the next step.
4. The apparent position of the asteroid is recalculated with a higher accuracy, taking account of the correction for the light-time, the gravitational deflection of light, the stellar aberration, and the precession and nutation of the Earth's rotational axis. It takes a long computation time to use this process, and thus the calculation is made only for events tentatively associated with an asteroid in the previous step.
5. The revised position of the asteroid is compared again with the position of the corresponding event. If the asteroid is located within 7.″5, the position match is regarded as being sufficient and the process goes to the next step.
6. Then, we check the predicted V-band magnitude (M_V) of the asteroid at the observation epoch. If the predicted M_V is too faint, the asteroid should not have been detected with AKARI and the identification is regarded as being false. M_V is calculated by using the formulation of Bowell et al. (1989) with the calculated heliocentric distance, "AKARI-centric" distance, the absolute magnitude (H), and the slope parameter (G). These H–G values are taken from the data set of Lowell Observatory as the same file as the orbital elements. These data mainly originate with the Minor Planet Center.

   At the same time, the rate of change in right ascension and declination seen from AKARI, the elongations of the Sun and the Moon, the phase angle (angle Sun-asteroid-AKARI), and the galactic latitude are calculated for later processes.

   If M_V of the object is brighter than 23 mag, the event is concluded to be associated with an asteroid. Otherwise the event is discarded.

It should be noted that the 2.′5 threshold of the position difference in step 3 is determined as the maximum value of the correction for the light-time, assuming a virtual asteroid with the moving speed of $11000'\,\mathrm{hr}^{-1}$ at 0.1 AU from the observer, as

$$\frac{11000}{3600}('\,\mathrm{s}^{-1}) \times 0.1\,(\mathrm{AU}) \times 499.005(\mathrm{s\,AU}^{-1}) \sim 2.'5,$$

and that the 7.″5 threshold in step 5 is determined as covering the signal shifted by 1 pixel on the detector by chance, where the pixel scale of the detector is 2.″3; the FWHM of the point source is 5.″5,[3] and the position uncertainty including the corrections in step 4 is assumed to be less than 1″.

2.2.3. Color correction and removal of spurious identification

Differences in color between asteroids and the calibration stars used in the IRC-PSC (mainly K- and M-giants, Ishihara et al. 2010) are not negligible because of the wide bandwidths of *S9W* and *L18W* and the continuum spectra in asteroids that cannot be assumed as being perfect blackbody or graybodies. Therefore, we empirically and approximatly express the color-correction factor as a polynomial function of the heliocentric distance of the object,

$$F_{\mathrm{cc}} = \frac{F_{\mathrm{raw}}}{E_{\mathrm{ccf}}} \tag{1}$$

and

$$E_{\mathrm{ccf}} = a_0 + a_1 R_{\mathrm{h}} + a_2 R_{\mathrm{h}}^2 + a_3 R_{\mathrm{h}}^3\,, \tag{2}$$

where F_{cc}, F_{raw}, E_{ccf}, and R_{h} are the color-corrected monochromatic flux at 9 or 18 μm, the raw in-band flux, the color correction factor, and the heliocentric distance, respectively. This formula is evaluated using the predicted thermal flux and the relative spectral response functions of the *S9W* and *L18W* bands. The predicted thermal flux is calculated

Table 2. Coefficients of the color correction factors.

	a_0	a_1	a_2	a_3
S9W	0.984	−0.068	0.031	−0.0019
L18W	0.956	−0.024	0.007	−0.0003

assuming that a virtual asteroid with $d = 100$ km and $p_v = 0.1$ is located at a heliocentric distance of between 1.0–6.0 AU with a step of 0.05 AU, where d and p_v are the size (diameter) and the geometric albedo, respectively. We determined the coefficients a_0, a_1, a_2, and a_3, as listed in table 2. The fitting errors of equation (2) to the calculated-model flux are 6% for *S9W* and 2.5% for *L18W* at most. The actual values of $1/E_{ccf}$ are in ranges of 1.06–0.80 for *S9W* and 1.07–0.99 for *L18W* for a heliocentric distance of 1–6 AU.

Up to this stage, the flux level of each event has not been taken into account in the identification procedure. We discard false identifications in the following steps based on the flux level:

- Events with extremely large uncertainties in the flux are discarded. Here, we set the threshold of the flux uncertainty at 71 Jy for *S9W* and at 96Jy for *L18W*. These threshold values are determined by the 5σ clipping method; i.e., the standard deviation (σ) of distribution of flux uncertainties for all events is determined and the event of the outside of the 5σ value is discarded; 47 events at *S9W* and 101 at *L18W* are discarded on these criteria. In fact, this step efficiently excludes events affected by the stray light near the Moon.
- The faintest sources in the IRC-PSC have fluxes of 0.045 Jy at *S9W* and 0.06 Jy at *L18W* (Ishihara et al. 2010). These values correspond to signal-to-noise ratios (S/N) of 6 and 3, respectively. There are a few events of which fluxes are fainter than these values in the event list. Because of the low S/N of the fluxes, it is difficult to accurately derive the size and albedo of these objects. Thus, these objects are also excluded from the catalog.

2.2.4. *Thermal model calculation*

Radiometric analysis of the identified events was carried out with the calibrated, color-corrected, monochromatic fluxes described in sub-subsection 2.2.3. We used a modified version of the Standard Thermal Model (STM: Lebofsky et al. 1986). In the STM, it was assumed that an asteroid is a nonrotating, spherical body, and the thermal emission from the point on an asteroid's surface is instantaneously in equilibrium with the solar flux absorbed at that point. Then, the temperature distribution, T, on a smooth spherical surface of asteroid was simply assumed to be symmetric with respect to the subsolar point as:

$$T(\varphi) = \begin{cases} T_{SS}\cos^{1/4}\varphi\,, & \text{for} \quad \varphi \le \pi/2\,, \\ 0\,, & \text{for} \quad \varphi > \pi/2\,, \end{cases} \tag{3}$$

where φ is the angular distance from the subsolar point. This assumes that the temperature on the nightside is treated as zero. The subsolar temperature, T_{SS}, is determined by equating the energy balance so that the absorbed sunlight is instantaneously re-emitted at thermal infrared wavelengths; thus,

$$T_{SS} = \left[\frac{(1-A_B)S_s}{\eta\varepsilon\sigma R_h^2}\right]^{1/4}, \tag{4}$$

where A_B, S_s, η, ε, and σ are the Bond albedo, the incident solar flux, the beaming parameter, the infrared emissivity, and the Stefan–Boltzmann constant, respectively. It is usually assumed that

$$A_B = q p_v\,, \tag{5}$$

where q and p_v are the phase integral and the geometric albedo. The phase integral, q, is given (the standard H–G system: Bowell et al. 1989) by

$$q = 0.290 + 0.684\,G\,, \tag{6}$$

where G is the slope parameter.

The scattered light is observed at optical to near-infrared wavelengths. The diameter can then be derived from the relation as

$$d = \frac{1329}{\sqrt{p_v}}\,10^{-H/5}, \tag{7}$$

where d and H are the diameter in units of km and the absolute magnitude, respectively (see, e.g., Fowler & Chillemi 1992).

In applying the STM, the parameters H and G, which are used in the identification process (sub-subsection 2.2.2), are also employed as an optical flux. The infrared emissivity, ε, is assumed to be a constant of 0.9 as a standard value for the mid-infrared. The geometry is determined by the heliocentric distance, the AKARI-centric distance, and the phase angle. We assume a thermal infrared phase coefficient of 0.01 mag deg^{-1} as specified for the STM. For the error calculation, we assign uncertainties of 0.05 mag for H and 0.02 for G. While the beaming parameter, η, basically accounts for the physical quantities relating to the surface roughness and the thermal inertia of the asteroid, it is used just as an empirical parameter, particularly in the STM.

The thermal flux of the model is calculated by integrating the Planck function numerically using equation (3) over a spherical asteroid of the diameter d under the condition of equation (7). The process is iteratively examined until the model flux converges on the observed value by adjusting the variables d and p_v.

In the first analysis we concentrated on 55 selected, well-studied main-belt asteroids (Müller et al. 2005), whose size, shape, rotational property, and albedo are known from different measurements (occultation, direct imaging, flybys, and radiometric techniques based on large thermal data sets), as listed in table 11 in appendix 2. These samples included asteroids having sizes of between ~ 70 and 1000 km and albedos of from 0.03 to 0.4. The verification of the STM approach for a given AKARI asteroid was examined with this data set. Lebofsky et al. (1986) did a similar exercise for 1 Ceres and 2 Pallas and derived a beaming parameter of $\eta = 0.756$ to obtain an acceptable match between the radiometrically derived size and albedo from N- and Q-band fluxes of ground-based observations and the published occultation diameters. For the AKARI data set of *S9W* and *L18W*, we adjusted the beaming parameter to obtain the best fit in the size and albedo between the values derived from the AKARI 2-band data and the known values. The best

fit was obtained with $\eta = 0.87$ for *S9W* and 0.77 for *L18W*. We also attempted to fit the 2-band data simultaneously with a single η for those objects for which both data were available at the same epoch. However the overall match became significantly worse. We therefore decided to use different values of η for each band.

2.2.5. Final adjustment and creation of the catalog

Thermal model calculations provide unreasonable values (either too bright or too dark) for some asteroids. They are regarded as false identification. We set the threshold of albedo at $0.01 < p_v < 0.9$ and those being outside the range were discarded. The number of the discarded events at this stage was 178 for *S9W* and 53 for *L18W*, $\sim 1\%$ of the total identified events.

To obtain the final product, we took means of the size and albedo with the weight of the S/N for each object. For the IRC All-Sky Survey data, the S/N is given as a function of the measured flux (see figure 15 in Ishihara et al. 2010). For the asteroids, $\sim 68\%$ of *S9W* and 74% of *L18W* events reach the maximum S/N values, $S/N = 15$ for *S9W* and $S/N = 18$ for *L18W*. The corresponding flux is ~ 0.6 Jy at *S9W* and ~ 1.0 Jy at *L18W*. If all the fluxes of an asteroid are above these values, the weighted mean is equal to a simple arithmetic mean.

Finally, a total of 5120 objects (5079 numbered and 41 unnumbered asteroids) were included in the catalog of the AKARI Mid-infrared Asteroid Survey, named the Asteroid Catalog Using AKARI (AcuA).

3. Evaluation of the Asteroid Catalog

3.1. Uncertainty of the Catalog Data

One of the major contributions that cause uncertainties in the size and albedo is the uncertainty of the observed fluxes of the asteroids. It is expressed in terms of the S/N of the fluxes of the events in the IRC-PSC. As mentioned in subsubsection 2.2.5, the S/N reached a plateau at $S/N = 15$ for *S9W* and $S/N = 18$ for *L18W*. Thus, even for the best cases the uncertainties in the fluxes for *S9W* and *L18W* are 6.7% and 5.6%, respectively. These directly resulted in uncertainties in the size of 3.3% and 2.8% and in the albedo of 6.7% and 5.6%. It was inherent component in this work.

The absolute magnitude (H) was adopted from the same data set of Lowell Observatory, as the orbital elements described in sub-subsection 2.2.2. The uncertainty in H is given as three levels: 0.5, 0.05, and 0.005 mag in the data set. We suspect that H has a large uncertainty, and is probably larger than those cataloged in some cases. Thus, we decided to give a constant uncertainty of 0.05 mag for those objects listed with uncertainties of 0.005 mag (963 asteroids) and 0.05 mag (4157 asteroids) of our 5120 cataloged asteroids, rather than using the original uncertainties in the data set. This corresponds to a 4.6% uncertainty in albedo and less in size. The slope parameter (G) was also taken from the data set of Lowell Observatory. In our cataloged asteroids, 5015 objects were assumed as $G = 0.15$, and others were provided severally. The uncertainty of G was assumed to be 0.02 uniformly. It has a small influence on the derived size and albedo, as expected in equation (6).

In our catalog, these three parameters, i.e., the observed fluxes, the absolute magnitude H and the slope parameter G are considered as the contributed factors for the uncertainties in the size and albedo. From these combinations, a typical value of uncertainties in size is 4.7%, and that in albedo is 10.1%. The other components discussed below were not used for the uncertainty calculation, because they were not appropriately quantified in this work.

In this work, we applied the STM (sub-subsection 2.2.4) to derive the size and albedo. It is assumed that an asteroid is a nonrotating, spherical body at a limit of zero thermal inertia. Thus, the flux variation due to rotation of an object was neglected. Detailed investigations require further information on the object, such as the individual shape model, the direction of the spin vector, and so forth. Since continuous observations with AKARI have at least a 100 min interval (one orbital period of the satellite) inevitably, light curves with fine time resolution cannot be obtained. Therefore, it is difficult to determine the detailed model parameters solely by AKARI observations. It is known that many asteroids have large amplitude ($\sim 30\%$) in the light curves (Warner et al. 2009). This adds $\sim 3\%$–$\sim 10\%$ uncertainties in size, especially for asteroids with a small number of detections. Therefore, the uncertainties in the size and albedo originating from the flux uncertainty could be larger for those asteroids.

The model parameters in the STM are the emissivity (ε), the thermal infrared phase coefficient, and the beaming parameter (η). The first two parameters are given as fixed values in advance. Because of a severe constraint on the solar elongation, it is difficult to make observations with AKARI from several different phase angles. For this reason, the phase coefficient was fixed at 0.01 mag deg^{-1} in the present analysis (Matson 1971). Different values were used for the beaming parameter, η, for *S9W* and *L18W*. The different values were chosen to adjust the derived size and albedo to those reported in previous works. The failure of the single value of η to provide good results in previous works may stem from the invalid assumptions in the STM. The beaming parameter is in fact not a physical quantity, but rather introduced to account for the observation empirically. AKARI did not observe an asteroid with the two bands simultaneously, which could affect the way of the adjustment of η at the two bands. The uncertainty of η, a 5% change in η, leads to $\sim 4\%$ at *S9W* and $\sim 2\%$ at *L18W* in size and $\sim 8\%$ at *S9W* and $\sim 5\%$ at *L18W* in albedo, depending slightly on the albedo of the object.

The geometry is given by the heliocentric distance, the AKARI-centric distance, and the phase angle. These are dependent on the position accuracy of the IRC-PSC (less than $2''$: Ishihara et al. 2010), and the uncertainties of the obtained catalog values are negligible.

3.2. Total Number and Spatial Distribution

The number of asteroids identified in the AKARI All-Sky Survey is summarized in table 1. The net number of the asteroids detected with *S9W* and *L18W* in total is 5120. The number of asteroids detected at *L18W* is larger than that at *S9W* by about twice. The number of the point sources detected at *S9W* in the IRC-PSC is approximately four times as many as that at *L18W*. The opposite trend can be explained by the different spectral energy distribution of the objects; asteroids

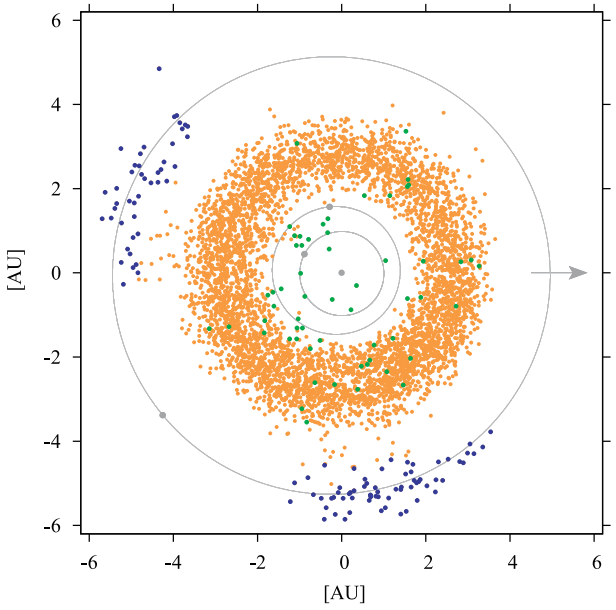

Fig. 4. Distribution of the identified asteroids projected on the plane of the ecliptic as of 2006 February 22. The circles indicate the orbits of the Earth, Mars, and Jupiter from inside to outside. The orange, green, and blue dots indicate the main-belt asteroids, the near-Earth asteroids, and the Jovian Trojans, respectively. The arrow shows the direction of the vernal equinox.

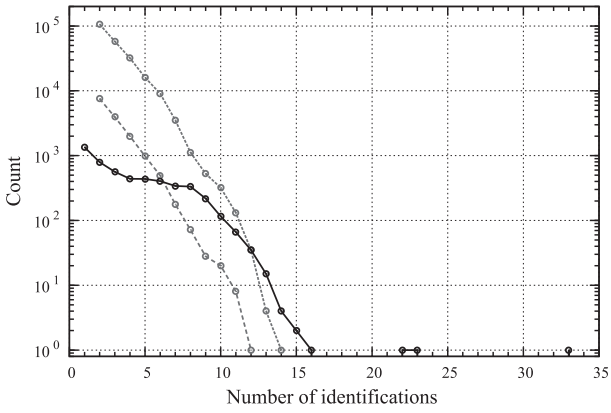

Fig. 5. Histogram of the number of detections of the asteroids identified with the AKARI All-Sky Survey (solid line). The objects with extremely large numbers are 137805 (1999 YK5) with 33 detections, P/2006 HR30 (Siding Spring) with 23, 85709 (1998 SG36) with 22, and 366 Vincentina (1893 W) with 16. The gray dashed and the gray dotted lines show the numbers of events with the sum of *S9W* and *L18W*, which are used as input to the IRC-PSC,[3] for $|\beta| < 1°$ and $|\beta| < 15°$, respectively, where β is the ecliptic latitude of the source.

have typical effective temperatures of around 200 K and radiate thermal emission with a peak wavelength of $\sim 15\,\mu$m, which can preferentially be detected at *L18W*, even if the difference in the sensitivity is taken account (figure 2). Stellar sources emit radiation with the peak wavelength at UV to optical, and are thus detected with a higher probability at *S9W*. A significant fraction of asteroids, particularly in the main-belt rather than the near-Earth, are detected only at *L18W*, but undetected at *S9W* because of the steep decrease in the thermal radiation in Wien's domain.

In figure 4, we show the distribution of the identified asteroids projected on the plane of the ecliptic (i.e., the face-on view). The near-Earth asteroids, the main-belt asteroids, and the Jovian Trojans can be discerned in the plot, while Centaurs and Trans-Neptune objects were not detected in our survey. Figure 4 displays the location of the 5120 asteroids at the epoch of 2006 February 22. It shows the distribution of asteroids without any bias or survey gap.

3.3. *Number of Detections Per Asteroid*

Figure 5 illustrates the number of detections of each asteroid with the AKARI All-Sky Survey. For comparison, we also plotted the number of detections for the point sources in the IRC-PSC around the plane of the ecliptic, which included galactic and extragalactic objects. AKARI basically observes a given portion of the sky at least twice in contiguous scans. Hence, a point source should have been observed four times at *S9W* and *L18W* in total. Because the lifetime of the AKARI cryogenic mission phase was 550 d, it observed a given portion of the sky at three different seasons. Accordingly, AKARI should have observed a point source on the ecliptic 12 times on average. The number could decrease because of the disturbance due to the SAA and the Moon or increase by the offset survey described in subsection 2.1. For the solar-system objects, the situation becomes complicated due to their orbital motions. Considering the rate of change in the ecliptic longitude ($d\lambda/dt$), there are only five objects in the AKARI catalog of $1\farcm8\,\mathrm{hr}^{-1} < d\lambda/dt < 4\farcm0\,\mathrm{hr}^{-1}$: 137805 ($2\farcm96\,\mathrm{hr}^{-1}$), P/2006 HR30 ($3\farcm50\,\mathrm{hr}^{-1}$), 85709 ($2\farcm95\,\mathrm{hr}^{-1}$), 7096 Napier ($1\farcm93\,\mathrm{hr}^{-1}$), and 7977 ($2\farcm66\,\mathrm{hr}^{-1}$), while the scan path of the All-Sky Survey shifts at most by $\sim 2\farcm47\,\mathrm{hr}^{-1}$ ($= 360°\,\mathrm{yr}^{-1}$) in the ecliptic longitude (i.e., in the cross-scan direction). The orbits of these objects are illustrated in figure 6. These objects, except for 7977, have a large number of detections, e.g., more than 15 times, suggesting that they keep up with the scan direction: 33 times for 137805, 23 times for P/2006 HR30, 22 times for 85709, and 15 times for 7096 Napier. Although P/2006 HR30 is classified as a Halley-type comet (the Tisserand invariant value of $T_\mathrm{J} = 1.785$: Hicks & Bauer 2007) and its cometary activity is reported (Lowry et al. 2006), we include this object as an asteroid in this paper; 7977 has only 3 detections at *S9W*, due to interference with pointed observations as well as to the "negative" effect of the offset survey. 366 Vincentina has $d\lambda/dt = 0\farcm49\,\mathrm{hr}^{-1}$, which is out of the range of the "keep up" speed mentioned above, but it was observed 16 times. It has three observation opportunities, and at one of them (2006 November) the number of detections increased by the "positive" effect of the offset survey.

The present catalog contains only asteroids orbiting in the same direction as Earth and no asteroids with retrograde motion are included. The sources with multiple detections are generally more reliable in terms of the confirmation. The IRC-PSC only includes objects that are detected at the same position at least twice. The present catalog has 5120 asteroids with $N_\mathrm{ID} \geq 1$, and 3771 asteroids with $N_\mathrm{ID} \geq 2$, where N_ID is the number of events with *S9W* and *L18W* in total. It should be noted that the catalog includes asteroids with single detection

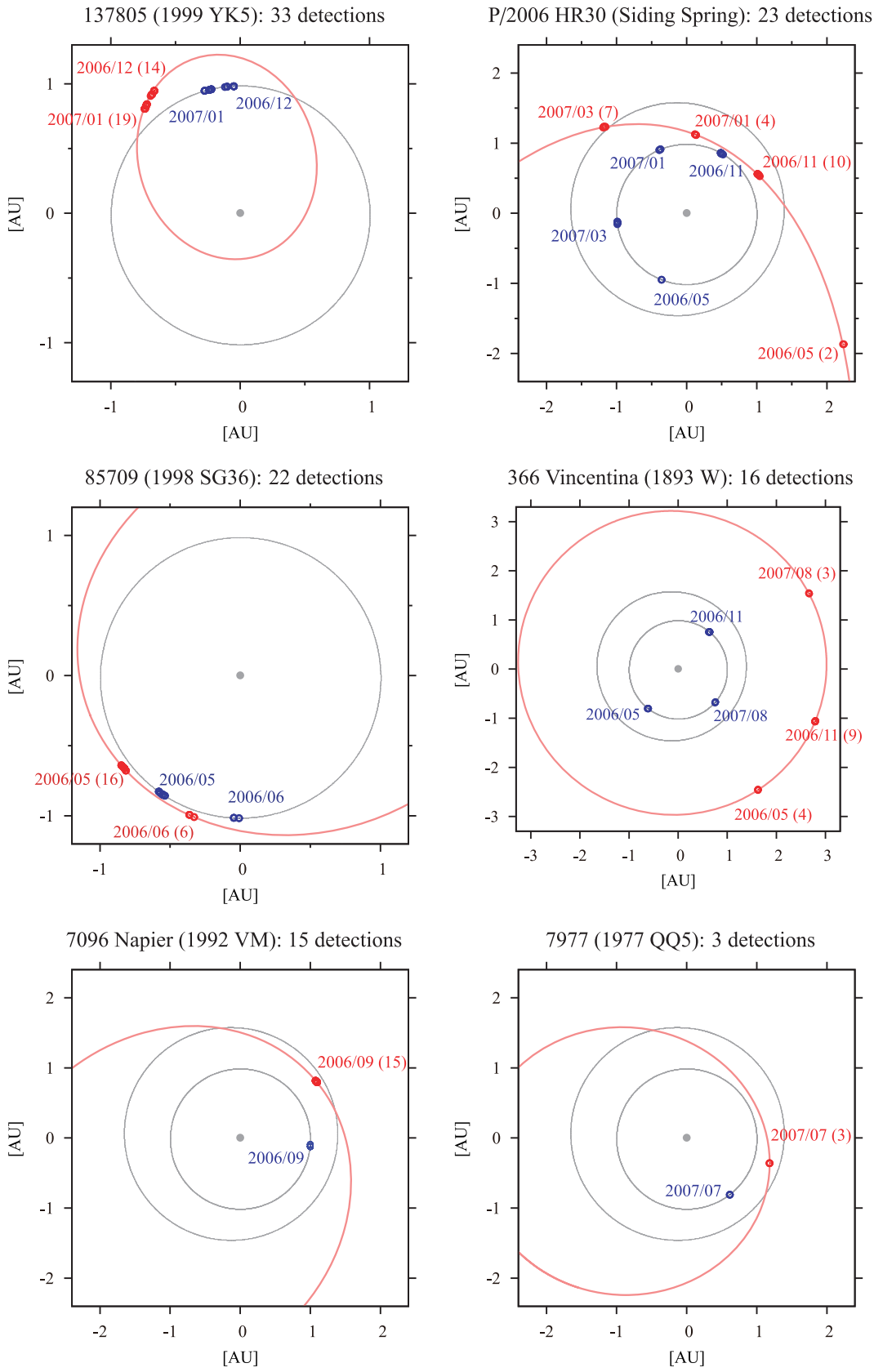

Fig. 6. Orbits of asteroids with a large number of detections projected on the plane of the ecliptic; 7977 is an exceptional case in this figure (only 3 detections, see text). The red and blue open circles indicate the positions of the asteroids in their orbit and those of Earth, respectively. The numbers of detections are given in the parentheses following the year/month of the observations. The orientation is the same as in figure 4, but the scale is different.

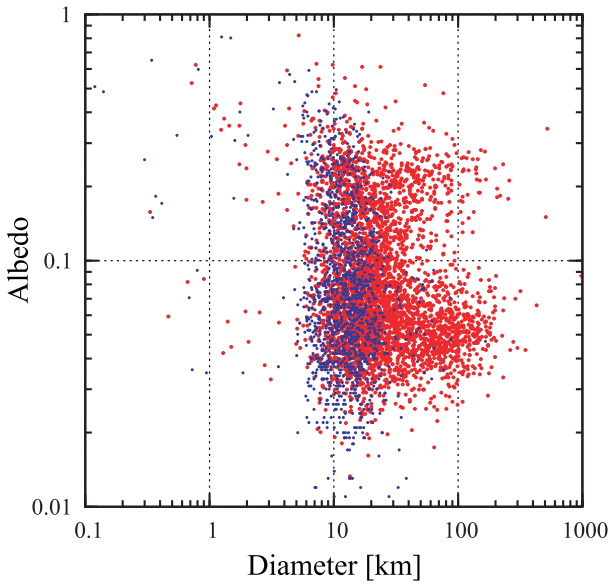

Fig. 7. Distribution of the size (diameter) and albedo of all the 5120 identified asteroids. Red dots show asteroids with more than two events, and blue ones indicate those with single-event detection.

($N_{\rm ID} = 1$). The number of detections is listed in the catalog (appendix 1).

3.4. Size and Albedo Distributions

Figure 7 shows the distribution of albedos as a function of the diameter for those asteroids detected with the AKARI All-Sky Survey. An outstanding feature is the bimodal distribution in the albedo. It is also suggested that the albedo increases as the size decreases for small asteroids ($d < 5$ km), although the number of asteroids with a size of $d < 5$ km is not large. In the catalog, the smallest asteroid is 2006 LD1, whose size is $d = 0.12 \pm 0.01$ km. The largest one is naturally 1 Ceres of $d = 970 \pm 13$ km.

Figure 8 illustrates histograms of the asteroids detected with the AKARI All-Sky Survey as a function of the size or the albedo. For comparison, the results of IRAS observations are also plotted. The IRAS catalog consists of 2228 objects with multiple detections and 242 objects with single detection (at the 12 μm band). It clearly indicates that the AKARI All-Sky Survey is more sensitive to small asteroids than IRAS. Concerning the size distribution of asteroids, the number is supposed to increase monotonically with the decrease of the size. Figure 8a, however, shows maxima at around $d = 15$ km for AKARI and 30 km for IRAS. The profiles of the histogram are similar to each other for those larger than 30 km, suggesting that IRAS and AKARI exhaustively detect asteroids of size $d > 30$ km and $d > 15$ km, respectively, but that the completeness rapidly drops for asteroids smaller than these values. We discuss further the size distribution in the following section. Figure 8b clearly indicates that the albedo of the asteroids has the well-known bimodal distribution (Morrison 1977b). The bimodal distribution can be attributed to two groups of taxonomic types of asteroids. The primary peak at around $p_{\rm v} = 0.06$ is associated with C and other low-albedo types, and the secondary peak at around $p_{\rm v} = 0.2$ with S and other types with moderate albedo. Further discussion concerning the taxonomic types will be presented in a forthcoming paper (F. Usui et al. in preparation).

3.5. V-Band Magnitude of the Identified Asteroids

Figure 9 shows the calculated V-band magnitude (M_V) against the color-corrected monochromatic flux of those events identified as asteroids; 3771 asteroids have multiple events in the AKARI All-Sky Survey. For example, 4 Vesta was observed with flux values of 134–139 Jy at *S9W* (2 times) and 474–604 Jy at *L18W* (3 times) with $M_V = 7.3$; 1 Ceres was observed with flux values of 127–142 Jy at *S9W* (3 times) and 497–853 Jy at *L18W* (4 times) with $M_V = 8.9$–9.0; 7 Iris was observed with flux values of 37–96 Jy at *S9W* (3 times) and 238–254 Jy at *L18W* (4 times) with $M_V = 9.3$–9.4. The bimodal characteristic is also seen in figure 9. A sharp cutoff of the flux below $\sim$0.1 Jy is the result of rejection of faint objects in the catalog processing (sub-subsection 2.2.3).

We set a threshold for M_V in the identification process (in step 6 in sub-subsection 2.2.2). Those objects of faintest M_V in figure 9 are 67999 (2000 XC32) with $M_V = 19.8$ at *S9W* and 102136 (1999 RO182) with $M_V = 20.3$ at *L18W*. It should be noted that both objects were observed only once in the AKARI All-Sky Survey. This result confirms that the threshold of $M_V = 23$ in sub-subsection 2.2.2 is reasonable to select real asteroids.

3.6. Detection Limit of the Size of Asteroids

Figure 10 shows the estimated size of the asteroids as a function of the heliocentric distance at the epoch of the AKARI observation. It is reasonable that smaller asteroids were detected more in near-Earth orbits. No asteroids were detected inside of the Earth orbit, because the viewing direction of AKARI was fixed at a solar elongation of $90° \pm 1°$. The smallest asteroids detected around the Earth orbit, the outer main-belt (3.27 AU), and Jupiter's orbit (5.2 AU, Trojans) were 0.1 km, 15 km, and 40 km, respectively.

3.7. Possibility of Discovery of New Asteroids

In asteroid catalog processing, we did not take into account the detection of new asteroids whose orbital parameters are not known. Reliable detection of unknown moving objects requires a high redundancy in the observations, which the AKARI All-Sky Survey did not provide. Unfortunately, the low visibility for observations around the plane of the ecliptic makes it difficult to reliably detect new asteroids solely from the AKARI All-Sky Survey database. However, it is also very likely that the AKARI All-Sky Survey database contains signals of undiscovered asteroids. In fact, we belatedly found that some asteroids had been detected with AKARI before their discovery. For instance, 2006 SA6, which was discovered on 2006 September 16 (Christensen et al. 2006), had been detected on 2006 June 25 with AKARI, and 2007 FM3, which was discovered on 2007 March 19 (Kowalski et al. 2007), had been observed on 2007 February 16 with AKARI (discoveries of these two were done by Catalina Sky Survey). Thus, whenever a new asteroid was discovered, we could check the detection in the AKARI All-Sky Survey database.

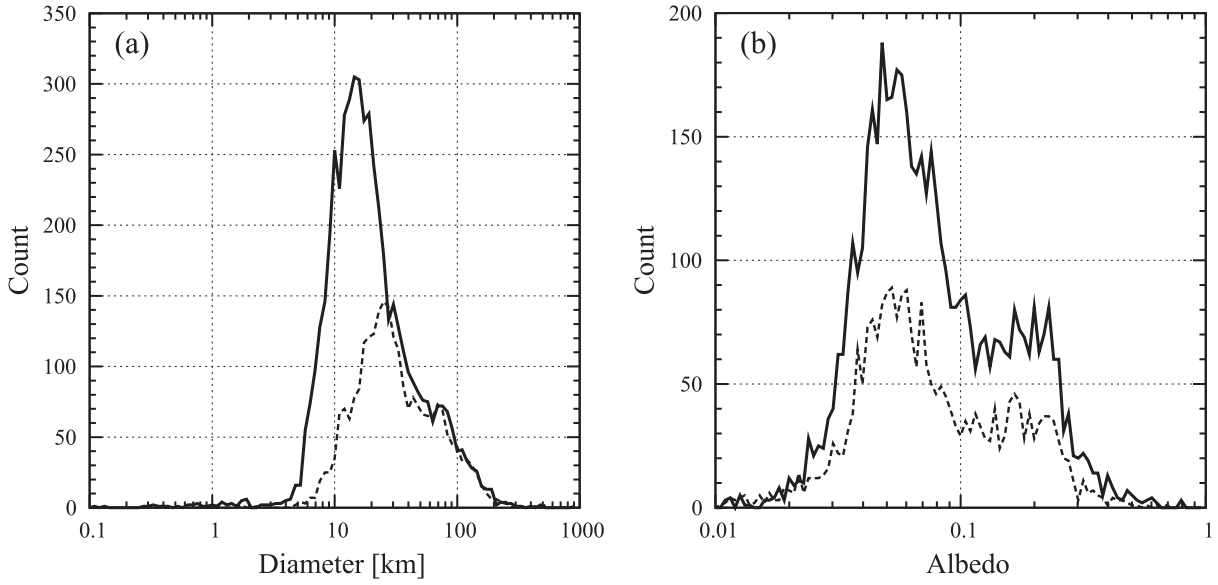

Fig. 8. Histograms of (a) the size (diameter) and (b) the albedo. The solid and dashed lines indicate the results from AKARI and IRAS observations (Tedesco et al. 2002a),[1] respectively. The bin size is set at 100 segments for the range of 0.1 km to 1000 km in the logarithmic scale for (a) and 100 segments for the range of 0.01 to 1.0 in the logarithmic scale for (b).

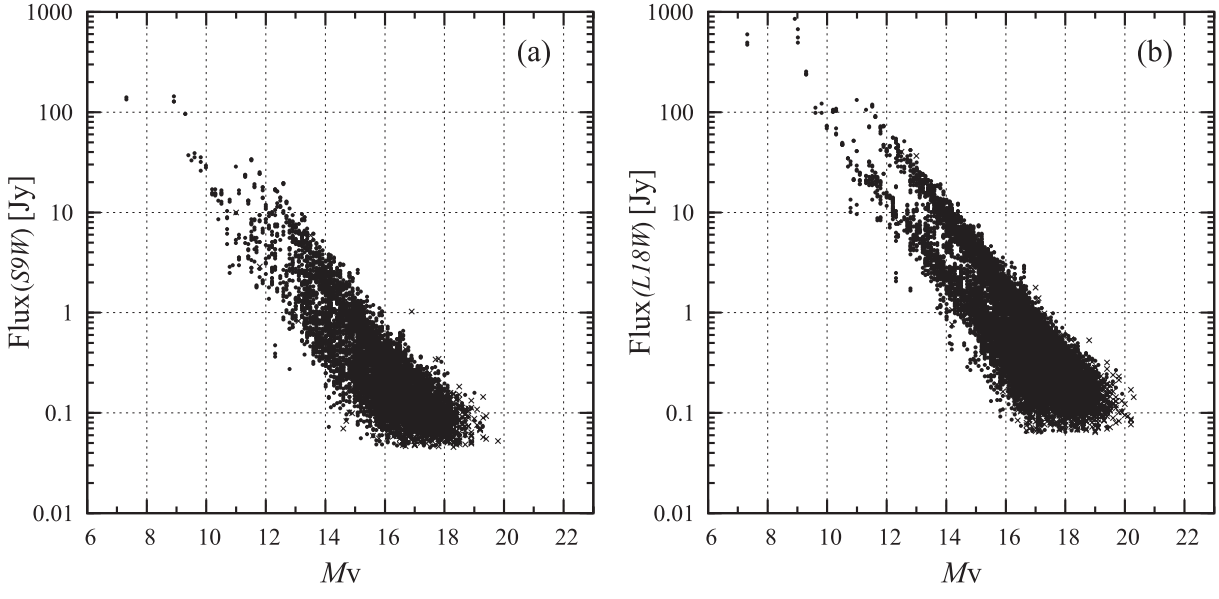

Fig. 9. Calculated V mag (M_V) vs. color-corrected (monochromatic) flux of the events identified as asteroids at (a) *S9W* and (b) *L18W*.

3.8. Comparison with Previous Works

3.8.1. Total Number of Detections

The total numbers of the detected asteroids with AKARI and previous works are summarized in table 3. The detected asteroids with AKARI are about twice as many as that with IRAS. A few hundred of asteroids were not detected with AKARI, which had been observed previously. Figure 11 shows the size distribution of the asteroids undetected with AKARI. Most observations of these asteroids were made with the Spitzer Space Telescope (SST) and with ground-based telescopes in programs to detect small asteroids. Figure 11 indicates that AKARI All-Sky Survey did not detect hundreds of small asteroids of $d < 15$ km due to the sensitivity limit.

3.8.2. Comparison with IRAS

Figure 12 shows a histogram of the asteroids detected with AKARI, without IRAS detection. A clear peak appears at around a size of $d \sim 15$ km, indicating that the AKARI All-Sky Survey extends the asteroid database down to $d \sim 15$ km. Table 4 lists large ($d > 100$ km) asteroids detected with

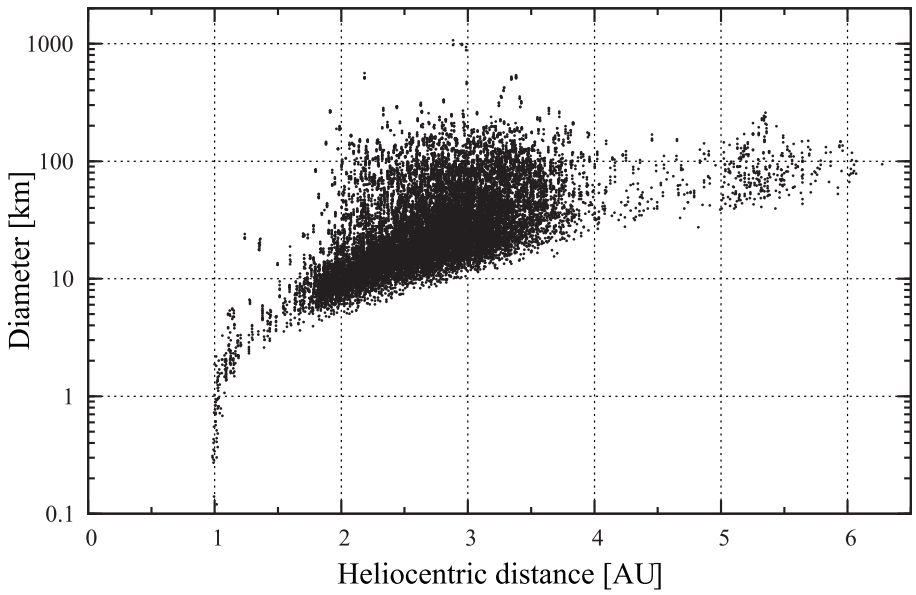

Fig. 10. Distribution of the estimated size (diameter) vs. the heliocentric distance of the detected asteroids at the epoch of the observation with AKARI.

Table 3. Number of asteroids with derived radiometric size/albedo information.*

	AKARI	IRAS	MSX	SST	Others
Asteroids with AKARI observations	5120	2103	160	7	288
Asteroids without AKARI observation	—	367	8	211	97
Total	5120	2470	168	218	385

* AKARI catalog compared to IRAS (Tedesco et al. 2002a),[1] MSX (Tedesco et al. 2002b),[2] SST (summarized in appendix 3:C1–C10), and other observations (in appendix 3:D1–D67).

Table 4. List of asteroids that were detected with AKARI, but undetected with IRAS ($d > 100$ km, 15 objects).†

Asteroid			Orbital elements			AKARI		Previous works		
			a[AU]	e	i [°]	d [km]	p_v	d [km]	p_v	References
624	Hektor	1907 XM	5.23749517	0.02237543	18.181769	230.99 ± 3.94	0.034 ± 0.001	239.20	0.041	D45, D58
19	Fortuna		2.44236038	0.15765176	1.572523	199.66 ± 3.02	0.063 ± 0.002	201.70	0.064	D3, D5, D7, D16, D55
375	Ursula	1893 AL	3.12268315	0.10721155	15.949598	193.63 ± 2.52	0.049 ± 0.001	—	—	(*)
190	Ismene		3.98157898	0.16462886	6.166222	179.89 ± 3.64	0.051 ± 0.003	—	—	(*)
24	Themis		3.12872103	0.13118619	0.759515	176.81 ± 2.30	0.084 ± 0.003	176.20	0.084	D52, D55
9	Metis		2.38647903	0.12228869	5.574494	166.48 ± 2.08	0.213 ± 0.007	154.67	0.228	B1, D3, D5, D42, D52, D55
14	Irene		2.58571736	0.16721133	9.105428	144.09 ± 1.94	0.257 ± 0.009	155.00	0.170	D3, D5
884	Priamus	1917 CQ	5.16616811	0.12330089	8.925189	119.99 ± 2.13	0.037 ± 0.001	138.00	0.034	D45
129	Antigone		2.86777878	0.21205688	12.218688	119.55 ± 1.42	0.185 ± 0.005	115.00	0.187	D7
275	Sapientia		2.77846168	0.16053249	4.768788	118.86 ± 1.76	0.036 ± 0.001	—	—	(*)
3451	Mentor	1984 HA1	5.10303310	0.07129302	24.695344	117.91 ± 3.19	0.075 ± 0.005	122.20	0.052	D45
127	Johanna		2.75462967	0.06479782	8.241708	114.19 ± 1.52	0.065 ± 0.002	123.33	0.056	B1
27	Euterpe		2.34596656	0.17303724	1.583754	109.79 ± 1.54	0.234 ± 0.008	118.00	0.110	D3, D5
481	Emita	1902 HP	2.74051861	0.15484764	9.837640	103.53 ± 1.90	0.061 ± 0.003	113.23	0.050	B1
505	Cava	1902 LL	2.68527271	0.24493942	9.839062	100.55 ± 1.24	0.063 ± 0.002	115.80	0.040	D55

† The parameters d, p_v, a, e, and i indicate the size (diameter), the albedo, the semimajor axis, the eccentricity, and the inclination of the asteroids, respectively. The references are summarized in appendix 3. The cited data refer to the underlined reference in the list. For those with the asterisks — that is, 375 Ursula, 190 Ismene, and 275 Sapientia — the AKARI data provide the first determination of the size and albedo.

Table 5. List of asteroids that were detected with IRAS and not with AKARI ($d > 40$ km, 11 objects).*

Asteroid			Orbital elements			Previous work		
			a [AU]	e	i [°]	d [km]	p_v	Reference
22180		2000 YZ	5.19497082	0.07172030	29.276964	64.18	0.052	A1
18137		2000 OU30	5.13890227	0.01629281	7.655306	60.71	0.013	A1
5027	Androgeos	1988 BX1	5.30195674	0.06662613	31.450673	57.86	0.092	A1
5025		1986 TS6	5.20547347	0.07670562	11.022628	57.83	0.064	A1
14268		2000 AK156	5.26980857	0.09197994	14.950850	57.54	0.037	A1
6545		1986 TR6	5.12777404	0.05220160	11.998200	56.96	0.055	A1
11542		1992 SU21	3.95030034	0.24086237	6.876531	49.72	0.022	A1
4317	Garibaldi	1980 DA1	3.98754535	0.16071342	9.823735	49.50	0.050	A1
13362		1998 UQ16	5.20935393	0.02839927	9.334905	48.21	0.048	A1
13035		1989 UA6	3.97417007	0.16620234	3.640840	47.40	0.018	A1
11351		1997 TS25	5.26120450	0.06567781	11.570297	42.16	0.063	A1

* The columns are the same as in table 4.

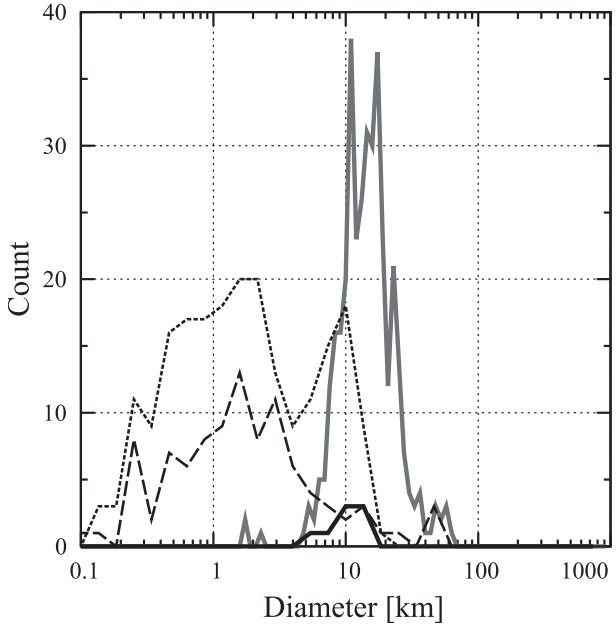

Fig. 11. Histogram of the asteroids with the previously determined size (diameter) without AKARI observation. The gray solid, black solid, black dotted, and black dashed lines indicate the data with IRAS, MSX, SST, and other observatories, respectively. The references are summarized in appendix 3. The bin size was set at 30 segments in the range of 0.1 km to 1000 km on the logarithmic scale, except for data with IRAS, for which the bin size was set at 100 segments.

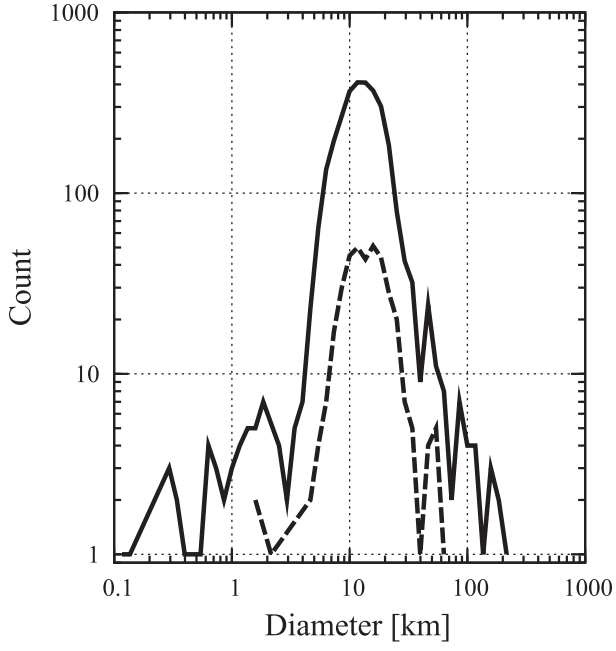

Fig. 12. Histogram of the size (diameter) of the asteroids determined by either AKARI or IRAS observations. The solid and dashed lines indicate the numbers of the asteroids that are detected with AKARI, but undetected with IRAS, and vice versa, respectively. The bin size was set at 60 segments in the range of 0.1 km to 1000 km on the logarithmic scale.

AKARI, but undetected with IRAS. Out of fifteen asteroids in this list, the size and albedo of the three asteroids [375 Ursula (1893 AL), 190 Ismene, and 275 Sapientia] were determined by our measurements for the first time. The size and albedo of the other twelve asteroids had been estimated with ground-based and space-borne telescopes previously. The AKARI asteroid catalog does not contain several very large ($d > 40$ km) asteroids detected with IRAS (table 5). For these asteroids, the size information was derived from IRAS observations. All of these asteroids are distant objects, and belong to the Jovian Trojans, except for the three Hildas: 11542 (1992 SU21), 4317 Garibaldi (1980 DA1), and 13035 (1989 UA6). The semimajor axes of these objects are larger than 3.9 AU. The closest heliocentric distances are ~ 5.1 AU for the Trojans and 4.4 AU for the Hildas during the period of the AKARI All-Sky Survey observation. The largest asteroid that AKARI failed to detect was 22180 (2000 YZ), whose size is $d = 64$ km according to IRAS observations. We examined the original scan data for these undetected large asteroids, and confirmed that two asteroids, 22180 (2000 YZ) and

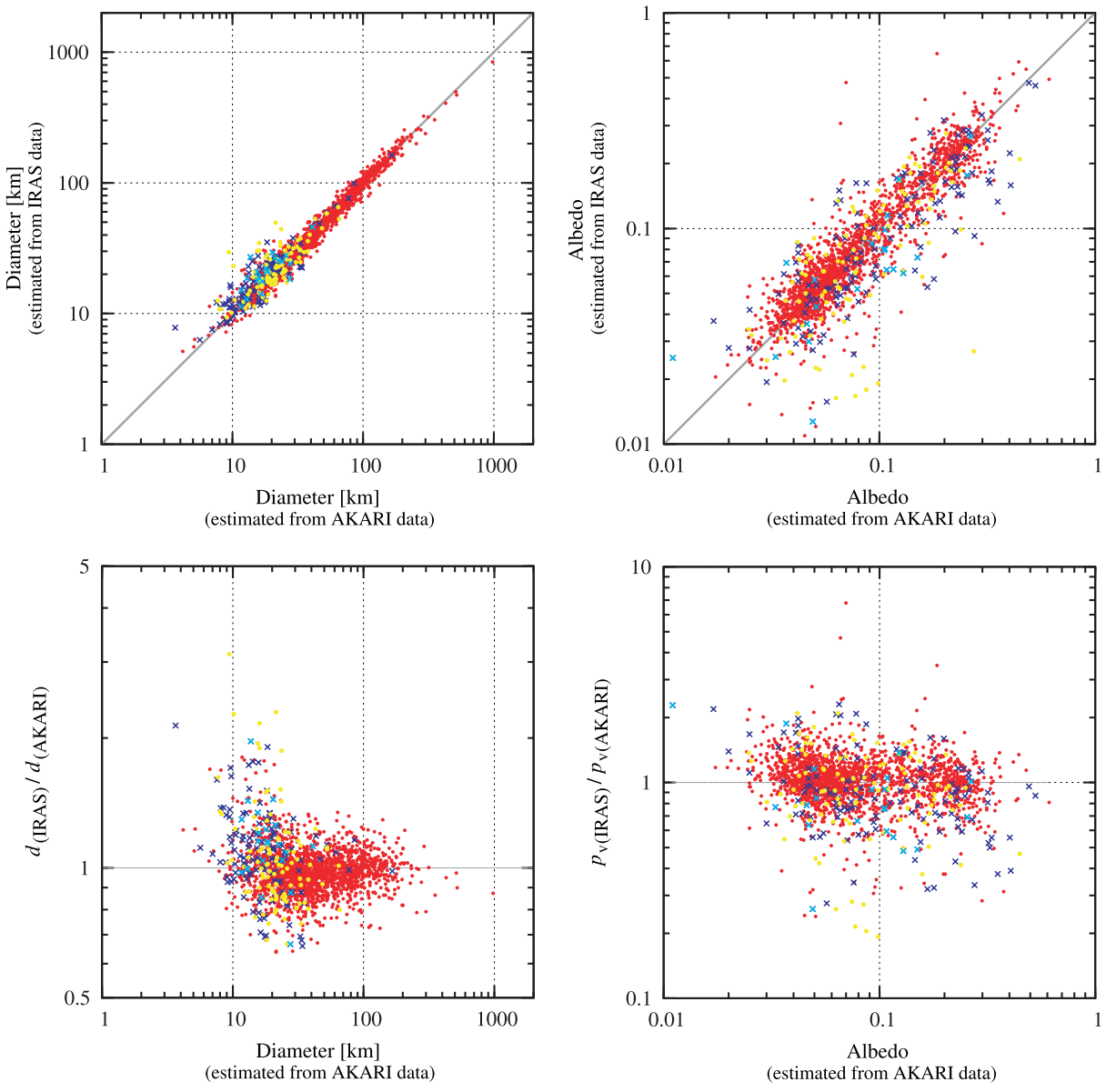

Fig. 13. Comparison between the estimates of AKARI and IRAS. The number of objects for each observation is shown in table 6. The red dot, the yellow dot, the blue cross, and the light-blue cross indicate the asteroids of (a), (b), (c), and (d) in table 6, respectively.

4317 (1980 DA1), can be seen in raw images of the All-Sky Survey data at *L18W* only once. They were, however, rejected because they were detected near to the edge of the detector. The other two asteroids, 14268 (2000 AK156) and 11542 (1992 SU21), are confused with stellar objects, since they are located at galactic latitudes of less than 1° at the epoch of the observation. For the other asteroids, no particular reasons for nondetection were found. Some of them may lose observation opportunities due to the offset survey operation mentioned in subsection 2.1. Deformed shapes, if any, may account for the nondetection with AKARI.

Figure 13 shows a comparison of the size and albedo of 2221 asteroids estimated from AKARI and IRAS observations (table 6). The AKARI measurement is fairly in agreement with

Table 6. Number of the asteroids for which the size and albedo were estimated with AKARI and IRAS observations.

		IRAS $N_{ID} \geq 2$	IRAS $N_{ID} = 1$
AKARI	$N_{ID} \geq 2$	1961 (a)	97 (b)
AKARI	$N_{ID} = 1$	142 (c)	21 (d)

* N_{ID} indicates the number of the observations. They are divided into four categories by $N_{ID} = 1$ or more with AKARI and IRAS (a, b, c, and d) as shown in figure 13.

Table 7. Asteroids that show large discrepancy in the size and albedo estimated from IRAS and AKARI observations.

Asteroid			IRAS data			AKARI data			Taxonomic	Family
			d [km]	p_v	N_{ID}*	d [km]	p_v	N_{ID}†	type	
(Asteroids with discrepant size)										
1293	Sonja	1933 SO	7.80	0.460	3	3.65 ± 0.45	0.529 ± 0.133	1	S	—
5356		1991 FF1	29.37	0.027	1	9.39 ± 0.70	0.273 ± 0.044	2	—	—
7875		1991 ES1	34.58	0.018	1	15.95 ± 0.45	0.087 ± 0.005	5	—	—
14409		1991 RM1	49.31	0.017	1	21.45 ± 0.88	0.077 ± 0.007	3	X(P)	—
16447	Vauban	1989 RX	23.10	0.019	1	10.17 ± 0.70	0.098 ± 0.014	2	—	—
(Asteroids with discrepant albedo)										
1166	Sakuntala	1930 MA	28.74	0.646	5	26.32 ± 0.39	0.185 ± 0.006	8	S	—
1384	Kniertje	1934 RX	27.51	0.308	8	26.14 ± 0.56	0.066 ± 0.003	7	C	Adeona
1444	Pannonia	1938 AE	29.20	0.475	2	30.48 ± 0.53	0.070 ± 0.003	7	C(B)	—
5661	Hildebrand	1977 PO1	34.37	0.136	2	42.29 ± 1.26	0.049 ± 0.003	5	—	Hilda

* The number of the observations used in the estimate of the albedo.
† The number of the detections with *S9W* and *L18W*.

Table 8. Summary for 5 taxonomic classes of the asteroids detected with AKARI.*

Taxonomic	AKARI			ECAS		
type	Number	$\overline{p_v}$	$\sigma(\overline{p_v})$	Number	$\overline{p_v}$	$\sigma(\overline{p_v})$
C	616	0.073	0.043	62	0.045	0.010
S	614	0.216	0.086	78	0.158	0.038
X	418	0.106	0.101	52	0.126	0.027
D	165	0.075	0.051	20	0.031	0.005
V	5	0.296	0.113	1	0.249	—
Total	1818			213		

* Current version of ECAS (Eight-Color Asteroid Survey)[6] contains not only the database of the reflectance spectrophotometric survey but also related data set including the geometric albedo which we refer to in this table.
The mean albedo is taken as the average value of the taxonomic classes that belong to the same taxonomic type, i.e., C-type: B, C, F, and G; S-type: A, Q, R, and S; X-type: X, M, and P; D-type: D and T; and V-type: V.
Determination of the taxonomic classes for AKARI samples is based on the references summarized in appendix 4: E1–E42.

the IRAS one. The correlation coefficients are 0.9895 for the size and 0.8978 for the albedo of the asteroids observed twice or more (1961 objects). However, there are large discrepancies in estimated size and albedo between several asteroids. We list these asteroids in table 7. The albedo of 1166 Sakuntala is estimated to be 0.65 from IRAS and 0.19 ± 0.01 from AKARI observations. Because this asteroid is classified as S-type, whose typical albedo is 0.216 [or 0.158 in the Eight Color Asteroid Survey (ECAS) data,[6] see table 8], an AKARI estimate is more likely to be correct. Two asteroids, 1384 Kniertje and 1444 Pannonia, have albedo values larger than 0.3 from IRAS, but ~ 0.07 from AKARI. Since these two asteroids are of C-type (the mean albedo of 0.073 or 0.045 in ECAS), IRAS observations seem to overestimate the albedo. The albedo of 5661 Hildebrand is estimated to be 0.14 from IRAS and 0.049 ± 0.003 from AKARI observations. Since this asteroid is a member of Hilda group, the Hildas, composed of D-type asteroids (Dahlgren & Lagerkvist 1995), which suggests the low albedo, the AKARI result seems to be more likely than the IRAS.

The discrepancy in the size estimate demands more detailed investigation. For 1 Ceres, the largest asteroid in the main belt or one of the dwarf planets, IRAS and AKARI estimate the size to be 850 km and 970 ± 13 km, respectively. Hubble Space Telescope observations (Thomas et al. 2005) derive it as 974.6×909.4 km, supporting the AKARI estimate. The 5 other asteroids listed in upper rows of table 7 only have sizes determined differently with IRAS and AKARI, and thus it is difficult to conclude which of the observations would be more accurate. Further observations and measurements are needed to understand the discrepancy in size between IRAS and AKARI.

[6] Eight Color Asteroid Survey V4.0, NASA Planetary Data System, EAR-A-2CP-3-RDR-ECAS-V4.0 ⟨http://sbn.psi.edu/pds/asteroid/ EAR_A_2CP_3_RDR_ECAS_V4_0/⟩.

Table 9. Format of the AKARI Asteroid Catalog.

Column	Format	Units	Label	Description
1– 6	A6	—	NUMBER	Asteroid's number
8–25	A18	—	NAME	Asteroid's name
27–36	A10	—	PROV_DES	Asteroid's provisional designation
38–42	F5.2	mag	HMAG*	Absolute magnitude
44–48	F5.2	—	GPAR*	Slope parameter
50–51	I2	—	NID	Number of detections by AKARI
53–59	F7.2	km	DIAMETER	Mean diameter
61–65	F5.2	km	D_ERR	Uncertainty in diameter
67–71	F5.3	—	ALBEDO	Mean geometric albedo
73–77	F5.3	—	A_ERR	Uncertainty in albedo

* The H–G values are taken from the Asteroid Orbital Elements Database of the Lowell observatory.

Table 10. Examples for the AcuA catalog data. The top 10 and bottom 10 asteroids in order of the number and provisional designation of asteroids are listed.

NUMBER	NAME	PROV_DES	HMAG [mag]	GPAR	NID	DIAMETER [km]	D_ERR [km]	ALBEDO	A_ERR
1	Ceres		3.34	0.12	7	973.89	13.31	0.087	0.003
2	Pallas		4.13	0.11	12	512.59	4.98	0.150	0.004
3	Juno		5.33	0.32	8	231.09	2.60	0.246	0.007
4	Vesta		3.20	0.32	5	521.74	7.50	0.342	0.013
5	Astraea		6.85	0.15	7	110.77	1.37	0.263	0.008
6	Hebe		5.71	0.24	11	197.15	1.83	0.238	0.006
7	Iris		5.51	0.15	7	254.20	3.27	0.179	0.006
8	Flora		6.49	0.28	10	138.31	1.37	0.235	0.006
9	Metis		6.28	0.17	7	166.48	2.08	0.213	0.007
10	Hygiea		5.43	0.15	6	428.46	6.57	0.066	0.002
⋮	⋮	⋮	⋮	⋮	⋮	⋮	⋮	⋮	⋮
		2006 SE285	16.43	0.15	1	3.56	0.30	0.037	0.006
		2006 UD185	14.39	0.15	3	8.76	0.42	0.048	0.005
		2006 UL217	20.72	0.15	1	0.14	0.01	0.487	0.073
		2006 VV2	16.79	0.15	1	1.03	0.03	0.318	0.024
		2006 WT1	19.99	0.15	1	0.35	0.02	0.150	0.018
		2007 AG	20.11	0.15	6	0.33	0.01	0.158	0.008
		2007 BT2	17.06	0.15	3	2.76	0.14	0.038	0.004
		2007 DF8	20.32	0.15	2	0.47	0.02	0.059	0.006
		2007 FM3	16.87	0.15	5	3.14	0.13	0.033	0.003
		2007 HE15	19.60	0.15	1	0.37	0.02	0.182	0.021

4. Concluding Remarks

We have created an unbiased, homogeneous asteroid catalog, which contains a total of 5120 objects. This is the second generation of asteroid surveys after the IRAS observation. The present catalog revises the properties of several asteroids. The catalog is publicly available via the Internet. This catalog will be significant for various fields of solar-system science, and contribute to future Rendezvous and/or sample return missions of small objects.

This study is based on observations with AKARI, a JAXA project with the participation of ESA. We would like to thank all members of the AKARI project for their devoted efforts to achieve our observations. We are grateful to I. Yamamura for kindly providing us with the computer environments, and also to A. Yoshino and the staffs of C-SODA, ISAS/JAXA for their steady arrangements of a web server for the public release of our catalog. Thanks are due to the referee, Simon Green, for his careful reading, and providing constructive suggestions, which have greatly helped to improve this paper. FU would like to thank C. P. Pearson for his helpful comments. SH is supported by the Space Plasma Laboratory, ISAS/JAXA. This work is supported in part by a Grant-in-Aid for Scientific Research on Priority Areas No.19047003 to DK, Grants-in-Aid for Young Scientists (B) No.21740153 and Scientific Research on

Table 11. Results of the STM calculation for the 55 selected asteroids.

Asteroid		Type	Detection with AKARI					Previous works		
			N_{ID} *S9W*	N_{ID} *L18W*	N_{ID} total	d [km]	p_v	d [km]	p_v	References
1	Ceres	C	3	4	7	973.89	0.087	959.60	0.096	A1, D2, D4, D5, D7, D8, D10, D16, D20, D26, D29, D33, D34, D42, D52, D67
2	Pallas	C	6	6	12	512.59	0.150	534.40	0.142	A1, D2, D5, D7, D15, D16, D20, D22, D26, D33, D42, D52, D67
3	Juno	S	4	4	8	231.09	0.246	233.92	0.238	A1, D2, D5, D26, D33, D42, D52
4	Vesta	V	2	3	5	521.74	0.342	548.50	0.317	A1, D1, D2, D3, D4, D5, D7, D8, D22, D25, D26, D33, D34, D42, D52, D67
6	Hebe	S	6	5	11	197.15	0.238	185.18	0.268	A1, D2, D16, D26, D34
7	Iris	S	3	4	7	254.20	0.179	199.83	0.277	A1, D3, D5, D15, D16, D26, D34, D42
8	Flora	S	4	6	10	138.31	0.235	135.89	0.243	A1, D3, D5, D26
9	Metis	D	4	3	7	166.48	0.213	154.67	0.228	B1, D3, D5, D42, D52, D55
10	Hygiea	C	3	3	6	428.46	0.066	469.30	0.056	A1, D3, D5, D16, D18, D22, D26, D33, D52, D67
12	Victoria	S	3	2	5	131.51	0.130	112.77	0.176	A1, D5, D7
17	Thetis	S	4	2	6	74.59	0.251	90.04	0.172	A1, D3, D5
18	Melpomene	S	3	3	6	139.95	0.225	140.57	0.223	A1, D3, D5, D34, D52
19	Fortuna	C	3	3	6	199.66	0.063	201.70	0.064	D3, D5, D7, D16, D55
20	Massalia	S	6	6	12	131.56	0.258	145.50	0.210	A1, D5, D7, D52
21	Lutetia	X	4	4	8	108.38	0.181	95.76	0.221	A1, D3, D5, D7, D59, D63
23	Thalia	S	1	3	4	106.21	0.260	107.53	0.254	A1, B1, D3, D5
24	Themis	C	4	4	8	176.81	0.084	176.20	0.084	D52, D55
28	Bellona	S	4	1	5	97.40	0.273	120.90	0.176	A1, B1, D5
29	Amphitrite	S	3	4	7	206.86	0.195	212.22	0.179	A1, D3, D5, D26
31	Euphrosyne	C	6	6	12	276.49	0.047	255.90	0.054	A1
37	Fides	S	3	3	6	103.23	0.204	108.35	0.183	A1, D3, D5
40	Harmonia	S	3	5	8	110.30	0.233	107.62	0.242	A1, D3, D5, D52
41	Daphne	C	3	4	7	179.61	0.078	174.00	0.083	A1, D7
42	Isis	S	4	3	7	104.50	0.158	100.20	0.171	A1, D7
47	Aglaja	C	2	1	3	147.05	0.060	126.96	0.080	A1, D5
48	Doris	C	3	4	7	200.27	0.077	221.80	0.062	A1
52	Europa	C	4	3	7	350.36	0.043	302.50	0.058	A1, D5, D7, D26
54	Alexandra	C	3	5	8	144.46	0.074	165.75	0.056	A1, D5, D7, D33, D52
56	Melete	X	4	6	10	105.22	0.076	113.24	0.065	A1, D5, D16
65	Cybele	X	4	2	6	300.54	0.044	237.26	0.071	A1, D16, D26, D33
69	Hesperia	X	5	4	9	132.74	0.157	138.13	0.140	A1
85	Io	C	4	4	8	150.66	0.071	154.79	0.067	A1, D7
88	Thisbe	C	3	4	7	195.59	0.071	200.58	0.067	A1
93	Minerva	C	3	3	6	147.10	0.068	141.55	0.073	A1, B1
94	Aurora	C	2	2	4	179.15	0.053	204.89	0.040	A1, D5, D7
106	Dione	C	3	3	6	153.42	0.084	146.59	0.089	A1, D7, D33
165	Loreley	C	4	2	6	173.66	0.051	154.78	0.064	A1
173	Ino	X	3	1	4	160.61	0.059	154.10	0.064	A1
196	Philomela	S	2	4	6	141.78	0.213	136.39	0.230	A1, D5, D7
230	Athamantis	S	4	5	9	108.28	0.173	108.99	0.171	A1, D3, D5, D7

Table 11. (Continued)

Asteroid	Type	Detection with AKARI					Previous works		
		N_{ID} *S9W*	N_{ID} *L18W*	N_{ID} total	d [km]	p_v	d [km]	p_v	References
241 Germania	C	3	3	6	181.57	0.050	168.90	0.058	A1, D5
283 Emma	C	4	8	12	122.07	0.039	148.06	0.026	A1
313 Chaldaea	C	4	4	8	94.93	0.054	96.34	0.052	A1, D5, D8, D33
334 Chicago	C	4	5	9	167.21	0.057	158.55	0.062	A1
360 Carlova	C	4	4	8	121.52	0.049	115.76	0.053	A1, D5, D7
372 Palma	C	2	4	6	177.21	0.075	188.62	0.066	A1
423 Diotima	C	5	1	6	226.91	0.049	208.77	0.051	A1
451 Patientia	C	5	5	10	234.91	0.071	224.96	0.076	A1, D5, D7, D16
471 Papagena	S	3	3	6	117.44	0.261	134.19	0.199	A1, D3
505 Cava	C	5	4	9	100.55	0.063	115.80	0.040	D55
511 Davida	C	4	3	7	290.98	0.070	326.06	0.054	A1, D2, D3, D7, D52
532 Herculina	S	4	2	6	216.77	0.184	222.39	0.169	A1, D3, D5, D8, D33, D42
690 Wratislavia	C	2	4	6	158.11	0.044	134.65	0.060	A1
704 Interamnia	C	7	4	11	316.25	0.075	316.62	0.074	A1, D5, D7,D52
776 Berbericia	C	4	5	9	149.76	0.067	151.17	0.066	A1

* The references of previous works are given in appendix 3. The cited data refer to the underlined reference in the list.

Innovative Areas No. 21111005 to TO, and a Grant-in-Aid for Scientific Research (C) No.19540251 to HK from the Ministry of Education, Culture, Sports, Science and Technology, and by a Grant-in-Aid for JSPS Fellows No.10J02063 to ST.

Appendix 1. Format of the AKARI/IRC Mid-Infrared Asteroid Survey

The Asteroid Catalog Using AKARI (AcuA) is publicly available on a web server[7] "Data ARchives and Transmission System (DARTS)" provided by Center for Science-satellite Operation and Data Archives (C-SODA) at the Institute of Space and Astronautical Science (ISAS), Japan Aerospace Exploration Agency (JAXA). It contains 5120 asteroids detected in the mid-infrared region along with the size, the albedo, and their associated uncertainties. It is in a standard ASCII file with a fixed-length record. Each line corresponds to each object with 10 columns. A summary of the format is given in table 9. NUMBER, NAME, and PROV_DES are the asteroid number, the name, and the provisional designation, which follow the formal assignment overseen by the IAU Minor Planet Center. HMAG and GPAR are the absolute magnitude and slope parameter taken from the Asteroid Orbital Elements Database of the Lowell observatory. NID gives the number of detections at *S9W* and *L18W* in total. DIAMETER and ALBEDO are the estimated size (diameter) and albedo, while D_ERR and A_ERR are their uncertainties estimated from the thermal model calculations. Users should note objects with single detection (NID = 1). Examples of the catalog data are given in table 10.

Appendix 2. List of 55 Asteroids Used for Thermal Model Calibration

We employed 55 well-studied main-belt asteroids (Müller et al. 2005) to derive the best value for the beaming parameter η (sub-subsection 2.2.4). Table 11 summarizes the calculation results of the 55 asteroids.

Appendix 3. Reference List of Previous Works of the Size and Albedo of Asteroids

The references of previous works are given in table 12.

Appendix 4. Reference List of Previous Works of the Taxonomic Types of Asteroids

The references of previous works used for determining the taxonomic classifications [based on the definitions by Tholen (1984), Bus (1999), and Lazzaro et al. (2004)] described in table 8 are given in table 12.

[7] ⟨http://darts.jaxa.jp/ir/akari/catalogue/AcuA.html⟩.

Table 12. List of references.

Size and albedo of asteroids		
Infrared Astronomical Satellite (IRAS):		
(A1) Tedesco et al. 2002a [1]		
Midcourse Space Experiment (MSX):		
(B1) Tedesco et al. 2002b [2]		
Spitzer Space Telescope (SST):		
(C1) Stansberry et al. 2008	(C5) Campins et al. 2009b	(C9) Bhattacharya et al. 2010
(C2) Trilling et al. 2008	(C6) Fernández et al. 2009	(C10) Trilling et al. 2010
(C3) Ryan et al. 2009	(C7) Harris et al. 2009	
(C4) Campins et al. 2009a	(C8) Licandro et al. 2009	
Other works including the Infrared Space Observatory (ISO) and ground-based observatories in the chronological order:		
1970–1979		
(D1) Allen 1970	(D5) Hansen 1976	(D9) Lebofsky et al. 1978
(D2) Cruikshank & Morrison 1973	(D6) Cruikshank & Jones 1977	(D10) Stier et al. 1978
(D3) Morrison 1974	(D7) Morrison 1977a	(D11) Lebofsky & Rieke 1979
(D4) Gillett & Merrill 1975	(D8) Gradie 1978	
1980–1989		
(D12) Lebofsky et al. 1981	(D16) Green et al. 1985a	(D20) Lebofsky et al. 1986
(D13) Brown & Morrison 1984	(D17) Green et al. 1985b	(D21) Tedesco & Gradie 1987
(D14) Lebofsky et al. 1984	(D18) Lebofsky et al. 1985	(D22) Johnston et al. 1989
(D15) LeVan & Price 1984	(D19) Vilas et al. 1985	(D23) Veeder et al. 1989
1990–1999		
(D24) Cruikshank et al. 1991	(D28) Campins et al. 1995	(D32) Jewitt & Kalas 1998
(D25) Redman et al. 1992	(D29) Altenhoff et al. 1996	(D33) Müller & Lagerros 1998
(D26) Altenhoff et al. 1994	(D30) Mottola et al. 1997	(D34) Redman et al. 1998
(D27) Altenhoff & Stumpff 1995	(D31) Harris et al. 1998	(D35) Harris & Davies 1999
2000–2009		
(D36) Thomas et al. 2000	(D47) Müller et al. 2004	(D58) Emery et al. 2006
(D37) Altenhoff et al. 2001	(D48) Cruikshank et al. 2005	(D59) Muller et al. 2006
(D38) Fernández et al. 2001	(D49) Fernández et al. 2005	(D60) Harris et al. 2007
(D39) Harris et al. 2001	(D50) Harris et al. 2005	(D61) Muller et al. 2007
(D40) Jewitt et al. 2001	(D51) Kraemer et al. 2005	(D62) Trilling et al. 2007
(D41) Fernández et al. 2002	(D52) Lim et al. 2005	(D63) Carvano et al. 2008
(D42) Müller et al. 2002	(D53) Müller et al. 2005	(D64) Hasegawa et al. 2008
(D43) Tedesco & Desert 2002	(D54) Rivkin et al. 2005	(D65) Wolters et al. 2008
(D44) Delbó et al. 2003	(D55) Tedesco et al. 2005 [9]	(D66) Delbo et al. 2009
(D45) Fernández et al. 2003	(D56) Wolters et al. 2005	(D67) Hormuth & Müller 2009
(D46) Delbó 2004[8]	(D57) Delbó et al. 2006	
Taxonomic types of asteroids		
(E1) Jewitt & Luu 1990	(E15) Le Bras et al. 2001	(E29) Lazzarin et al. 2005
(E2) Barucci & Lazzarin 1993	(E16) Manara et al. 2001	(E30) Marchi et al. 2005
(E3) Dahlgren & Lagerkvist 1995	(E17) Mothé-Diniz et al. 2001	(E31) Alvarez-Candal et al. 2006
(E4) Xu et al. 1995	(E18) Fornasier et al. 2003	(E32) Dotto et al. 2006
(E5) Dahlgren et al. 1997	(E19) Rivkin et al. 2003	(E33) de León et al. 2006
(E6) Di Martino et al. 1997	(E20) Yang et al. 2003	(E34) Michelsen et al. 2006
(E7) Lazzarin et al. 1997	(E21) Bendjoya et al. 2004	(E35) Davies et al. 2007
(E8) Doressoundiram et al. 1998	(E22) Binzel et al. 2004	(E36) Licandro et al. 2008
(E9) Hicks et al. 1998	(E23) Duffard et al. 2004	(E37) Moskovitz et al. 2008a
(E10) Hicks et al. 2000	(E24) Fornasier et al. 2004	(E38) Moskovitz et al. 2008b
(E11) Zappalà et al. 2000	(E25) Marchi et al. 2004	(E39) Mothé-Diniz & Nesvorný 2008a
(E12) Binzel et al. 2001	(E26) Lazzarin et al. 2004a	(E40) Mothé-Diniz & Nesvorný 2008b
(E13) Cellino et al. 2001	(E27) Lazzarin et al. 2004b	(E41) Roig et al. 2008
(E14) Fornasier & Lazzarin 2001	(E28) Lagerkvist et al. 2005	(E42) Duffard & Roig 2009

[8] ⟨http://sbn.psi.edu/pds/asteroid/EAR_A_KECK1LWS_ETAL_5_DELBO_V1_0/⟩.

[9] The actual data is avaliable at NASA Planetary Data System, Statistical Asteroid Model, Version 1.0 (SAM-I) ⟨http://sbn.psi.edu/pds/SAM-I/⟩.

References

Allen, D. A. 1970, Nature, 227, 158
Allen, D. A. 1971, in IAU Colloq. 12, Physical Studies of Minor Planets, ed. T. Gehrelsm, SP-267 (Washington, D.C.: NASA), 41
Altenhoff, W. J., Baars, J. W. M., Schraml, J. B., Stumpff, P., & von Kap-herr, A. 1996, A&A, 309, 953
Altenhoff, W. J., Johnston, K. J., Stumpff, P., & Webster, W. J. 1994, A&A, 287, 641
Altenhoff, W. J., Menten, K. M., & Bertoldi, F. 2001, A&A, 366, L9
Altenhoff, W. J., & Stumpff, P. 1995, A&A, 293, L41
Alvarez-Candal, A., Duffard, R., Lazzaro, D., & Michtchenko, T. 2006, A&A, 459, 969
Barucci, M. A., & Lazzarin, M. 1993, Planet. Space Sci., 41, 641
Bendjoya, P., Cellino, A., Di Martino, M., & Saba, L. 2004, Icarus, 168, 374
Bhattacharya, B., et al. 2010, ApJ, 720, 114
Binzel, R. P., Harris, A. W., Bus, S. J., & Burbine, T. H. 2001, Icarus, 151, 139
Binzel, R. P., Rivkin, A. S., Stuart, J. S., Harris, A. W., Bus, S. J., & Burbine, T. H. 2004, Icarus, 170, 259
Bottke, W. F., Jr., Durda, D. D., Nesvorný, D., Jedicke, R., Morbidelli, A., Vokrouhlický, D., & Levison, H. F. 2005, Icarus, 179, 63
Bowell, E., Hapke, B., Domingue, D., Lumme, K., Peltoniemi, J., & Harris, A. W. 1989, in Asteroids II, ed. R. P. Binzel et al. (Tucson: University of Arizona Press), 524
Bowell, E., Muinonen, K., & Wasserman, L. H. 1994, in Asteroids, Comets, Meteors 1993, ed. A. Milani et al. (Dordrecht: Kluwer Academic Publishers), 477
Britt, D. T., Yeomans, D., Housen, K., & Consolmagno, G. 2002, in Asteroids III, ed. W. F. Bottke Jr. et al. (Tucson: University of Arizona Press), 485
Brown, R. H., & Morrison, D. 1984, Icarus, 59, 20
Burbine, T. H., Rivkin, A. S., Noble, S. K., Mothé-Diniz, T., Bottke, W. F., McCoy, T. J., Dyar, M. D., & Thomas, C. A. 2008, Rev. Mineral. Geochem., 68, 273
Bus, S. J. 1999, PhD thesis, Massachusetts Inst. Technol.
Campins, H., Emery, J. P., Kelley, M., Fernández, Y., Licandro, J., Delbó, M., Barucci, A., & Dotto, E. 2009a, A&A, 503, L17
Campins, H., Kelley, M. S., Fernández, Y., Licandro, J., & Hargrove, K. 2009b, Earth, Moon, Planets, 105, 159
Campins, H., Osip, D. J., Rieke, G. H., & Rieke, M. J. 1995, Planet. Space Sci., 43, 733
Carvano, J. M., Barucii, M. A., Delbó, M., Fornasier, S., Lowry, S., & Fitzsimmons, A. 2008, A&A, 479, 241
Cellino, A., Zappalà, V., Doressoundiram, A., Di Martino, M., Bendjoya, Ph., Dotto, E., & Migliorini, F. 2001, Icarus, 152, 225
Christensen, E. J., et al. 2006, Minor Planet Electron. Circ., S16
Cruikshank, D. P., & Jones, T. J. 1977, Icarus, 31, 427
Cruikshank, D. P., & Morrison, D. 1973, Icarus, 20, 477
Cruikshank, D. P., Stansberry, J. A., Emery, J. P., Fernández, Y. R., Werner, M. W., Trilling, D. E., & Rieke, G. H. 2005, ApJ, 624, L53
Cruikshank, D. P., Tholen, D. J., Hartmann, W. K., Bell, J. F., & Brown, R. H. 1991, Icarus, 89, 1
Dahlgren, M., & Lagerkvist, C.-I. 1995, A&A, 302, 907
Dahlgren, M., Lagerkvist, C.-I., Fitzsimmons, A., Williams, I. P., & Gordon, M. 1997, A&A, 323, 606
Davies, J. K., Harris, A. W., Rivkin, A. S., Wolters, S. D., Green, S. F., McBride, N., Mann, R. K., & Kerr, T. H. 2007, Icarus, 186, 111
de León, J., Licandro, J., Duffard, R., & Serra-Ricart, M. 2006, Adv. Space Res., 37, 178
Delbo, M., Ligori, S., Matter, A., Cilino, A., & Berthier, J. 2009, ApJ, 694, 1228
Delbó, M. 2004, PhD thesis, Freie Universität Berlin
Delbó, M., et al. 2006, Icarus, 181, 618
Delbó, M., Harris, A. W., Binzel, R. P., Pravec, P., & Davies, J. K. 2003, Icarus, 166, 116
Di Martino, M., Migliorini, F., Zappalà, V., Manara, A., & Barbieri, C. 1997, Icarus, 127, 112
Doressoundiram, A., Barucci, M. A., Fulchignoni, M., & Florczak, M. 1998, Icarus, 131, 15
Dormand, J. R., El-Mikkawy, M. E. A., & Prince, P. J. 1987, IMA J. Numer. Anal., 7, 423
Dotto, E., et al. 2006, Icarus, 183, 420
Duffard, R., Lazzaro, D., Licandro, J., De Sanctis, M. C., Capria, M. T., & Carvano, J. M. 2004, Icarus, 171, 120
Duffard, R., & Roig, F. 2009, Planet. Space Sci., 57, 229
Emery, J. P., Cruikshank, D. P., & Van Cleve, J. 2006, Icarus, 182, 496
Fernández, Y. R., Jewitt, D. C., & Sheppard, S. S. 2001, ApJ, 553, L197
Fernández, Y. R., Jewitt, D. C., & Sheppard, S. S. 2002, AJ, 123, 1050
Fernández, Y. R., Jewitt, D. C., & Sheppard, S. S. 2005, AJ, 130, 308
Fernández, Y. R., Jewitt, D., & Ziffer, J. E. 2009, AJ, 138, 240
Fernández, Y. R., Sheppard, S. S., & Jewitt, D. C. 2003, AJ, 126, 1563
Fornasier, S., et al. 2003, A&A, 398, 327
Fornasier, S., Dotto, E., Marzari, F., Barucci, M. A., Boehnhardt, H., Hainaut, O., & de Bergh, C. 2004, Icarus, 172, 221
Fornasier, S., & Lazzarin, M. 2001, Icarus, 152, 127
Fowler, J. W., & Chillemi, J. R. 1992, Phillips Lab. Tech. Rep., 2049, 17
Gillett, F. C., & Merrill, K. M. 1975, Icarus, 26, 358
Gladman, B. J., et al. 2009, Icarus, 202, 104
Gradie, J. C. 1978, PhD thesis, Arizona University
Green, S. F., Eaton, N., Aitken, D. K., Roche, P. F., & Meadows, A. J. 1985a, Icarus, 62, 282
Green, S. F., Meadows, A. J., & Davies, J. K. 1985b, MNRAS, 214, 29
Hansen, O. L. 1976, AJ, 81, 74
Harris, A. W., & Davies, J. K. 1999, Icarus, 142, 464
Harris, A. W., Davies, J. K., & Green, S. F. 1998, Icarus, 135, 441
Harris, A. W., Delbó, M., Binzel, R. P., Davies, J. K., Roberts, J., Tholen, D. J., & Whiteley, R. J. 2001, Icarus, 153, 332
Harris, A. W., & Lagerros, J. S. V. 2002, in Asteroids III, ed. W. F. Bottke Jr. et al. (Tucson: University of Arizona Press), 205
Harris, A. W., Mueller, M., Delbó, M., & Bus, S. J. 2005, Icarus, 179, 95
Harris, A. W., Mueller, M., Delbó, M., & Bus, S. J. 2007, Icarus, 188, 414
Harris, A. W., Mueller, M., Lisse, C. M., & Cheng, A. F. 2009, Icarus, 199, 86
Hasegawa, S., et al. 2008, PASJ, 60, S399
Hicks, M. D., & Bauer, J. M. 2007, ApJ, 662, L47
Hicks, M. D., Buratti, B. J., Newburn, R. L., Jr., & Rabinowitz, D. L. 2000, Icarus, 143, 354
Hicks, M. D., Fink, U., & Grundy, W. M. 1998, Icarus, 133, 69
Hilton, J. L. 2002, in Asteroids III, ed. W. F. Bottke Jr. et al. (Tucson: University of Arizona Press), 103
Hormuth, F., & Müller, T. G. 2009, A&A, 497, 983
Ishihara, D., et al. 2010, A&A, 514, A1
Jewitt, D., Aussel, H., & Evans, A. 2001, Nature, 411, 446
Jewitt, D., & Kalas, P. 1998, ApJ, 499, L103
Jewitt, D. C., & Luu, J. X. 1990, AJ, 100, 933

Johnston, K. J., Lamphear, E. J., Webster, W. J., Jr., Lowman, P. D., Jr., Seidelmann, P. K., Kaplan, G. H., Wade, C. M., & Hobbs, R. W. 1989, AJ, 98, 335
Kawada, M., et al. 2007, PASJ, 59, S389
Kessler, M. F., et al. 1996, A&A, 315, L27
Kowalski, R. A., et al. 2007, Minor Planet Electron. Circ., F51
Kraemer, K. E., Lisse, C. M., Price, S. D., Mizuno, D., Walker, R. G., Farnham, T. L., & Mäkinen, T. 2005, AJ, 130, 2363
Lagerkvist, C.-I., Moroz, L., Nathues, A., Erikson, A., Lahulla, F., Karlsson, O., & Dahlgren, M. 2005, A&A, 432, 349
Lazzarin, M., Di Martino, M., Barucci, M. A., Doressoundiram, A., & Florczak, M. 1997, A&A, 327, 388
Lazzarin, M., Marchi, S., Barucci, M. A., Di Martino, M., & Barbieri, C. 2004a, Icarus, 169, 373
Lazzarin, M., Marchi, S., Magrin, S., & Barbieri, C. 2004b, Mem. Soc. Astron. Ital. Suppl., 5, 21
Lazzarin, M., Marchi, S., Magrin, S., & Licandro, J. 2005, MNRAS, 359, 1575
Lazzaro, D., Angeli, C. A., Carvano, J. M., Mothé-Diniz, T., Duffard, R., & Florczak, M. 2004, Icarus, 172, 179
Lebofsky, L. A., et al. 1985, Icarus, 63, 192
Lebofsky, L. A., et al. 1986, Icarus, 68, 239
Lebofsky, L. A., & Rieke, G. H. 1979, Icarus, 40, 297
Lebofsky, L. A., & Spencer, J. R. 1989, in Asteroids II, ed. R. P. Binzel et al. (Tucson: University of Arizona Press), 128
Lebofsky, L. A., Tholen, D. J., Rieke, G. H., & Lebofsky, M. J. 1984, Icarus, 60, 532
Lebofsky, L. A., Veeder, G. J., Lebofsky, M. J., & Matson, D. L. 1978, Icarus, 35, 336
Lebofsky, L. A., Veeder, G. J., Rieke, G. H., Lebofsky, M. J., Matson, D. L., Kowal, C., Wynn-Williams, C. G., & Becklin, E. E. 1981, Icarus, 48, 335
Le Bras, A., Dotto, E., Fulchignoni, M., Doressoundiram, A., Barucci, M. A., Le Mouélic, S., Forni, O., & Quirico, E. 2001, A&A, 379, 660
LeVan, P. D., & Price, S. D. 1984, Icarus, 57, 35
Licandro, J., et al. 2009, A&A, 507, 1667
Licandro, J., Alvarez-Candal, A., de León, J., Pinilla-Alonso, N., Lazzaro, D., & Campins, H. 2008, A&A, 481, 861
Lim, L. F., McConnochie, T. H., Bell, J. F., III, & Hayward, T. L. 2005, Icarus, 173, 385
Lowry, S. C., Fitzsimmons, A., Hicks, M. D., Lawrence, K., & Forti, G. 2006, IAU Circ., 8735
Manara, A., Covino, S., & Di Martino, M. 2001, Rev. Mex. Astron. Astrofis., 37, 35
Marchi, S., Lazzarin, M., & Magrin, S. 2004, A&A, 420, L5
Marchi, S., Lazzarin, M., Paolicchi, P., & Magrin, S. 2005, Icarus, 175, 170
Matson, D. L. 1971, in IAU Colloq. 12, Physical Studies of Minor Planets, ed. T. Gehrelsm, SP-267 (Washington, D.C.: NASA), 45
Michelsen, R., Nathues, A., & Lagerkvist, C.-I. 2006, A&A, 451, 331
Mill, J. D., et al. 1994, J. Spacecr. Rockets, 31, 900
Morrison, D. 1974, ApJ, 194, 203
Morrison, D. 1977a, ApJ, 214, 667
Morrison, D. 1977b, Icarus, 31, 185
Moskovitz, N. A., Jedicke, R., Gaidos, E., Willman, M., Nesvorný, D., Fevig, R., & Ivezić, Ž. 2008a, Icarus, 198, 77
Moskovitz, N. A., Lawrence, S., Jedicke, R., Willman, M., Haghighipour, N., Bus, S. J., & Gaidos, E. 2008b, ApJ, 682, L57
Mothé-Diniz, T., Di Martino, M., Bendjoya, P., Doressoundiram, A., & Migliorini, F. 2001, Icarus, 152, 117
Mothé-Diniz, T., & Nesvorný, D. 2008a, A&A, 486, L9
Mothé-Diniz, T., & Nesvorný, D. 2008b, A&A, 492, 593
Mottola, S., et al. 1997, AJ, 114, 1234
Muller, M., Harris, A. W., Bus, S. J., Hora, J. L., Kassis, M., & Adams, J. D. 2006, A&A, 447, 1153
Muller, M., Harris, A. W., & Fitzsimmons, A. 2007, Icarus, 187, 611
Müller, T. G., HERSCHEL Calibration Steering Group, and ASTRO-F Calibration Team 2005, in Proc. Dusty and Molecular Universe: A Prelude to Herschel and ALMA, ed. A. Wilson, ESA SP-577 (Noordwijk, Netherlands: ESA), 471
Müller, T. G., Hotzel, S., & Stickel, M. 2002, A&A, 389, 665
Müller, T. G., & Lagerros, J. S. V. 1998, A&A, 338, 340
Müller, T. G., Sekiguchi, T., Kaasalainen, M., Abe, M., & Hasegawa, S. 2005, A&A, 443, 347
Müller, T. G., Sterzik, M. F., Schütz, O., Pravec, P., & Siebenmorgen, R. 2004, A&A, 424, 1075
Murakami, H., et al. 2007, PASJ, 59, S369
Neugebauer, G., et al. 1984, ApJ, 278, L1
Onaka, T., et al. 2007, PASJ, 59, S401
Parker, A., Ivezić, Ž, Jurić, M., Lupton, R., Sekora, M. D., & Kowalski, A. 2008, Icarus, 198, 138
Price, S. D., Egan, M. P., Carey, S. J., Mizuno, D. R., & Kuchar, T. A. 2001, AJ, 121, 2819
Redman, R. O., Feldman, P. A., & Matthews, H. E. 1998, AJ, 116, 1478
Redman, R. O., Feldman, P. A., Matthews, H. E., Halliday, I., & Creutzberg, F. 1992, AJ, 104, 405
Rivkin, A. S., Binzel, R. P., & Bus, S. J. 2005, Icarus, 175, 175
Rivkin, A. S., Binzel, R. P., Howell, E. S., Bus, S. J., & Grier, J. A. 2003, Icarus, 165, 349
Roig, F., Nesvorný, D., Gil-Hutton, R., & Lazzaro, D. 2008, Icarus, 194, 125
Ryan, E. L., et al. 2009, AJ, 137, 5134
Stansberry, J., Grundy, W., Brown, M., Cruikshank, D., Spencer, J., Trilling, D., & Margot, J.-L. 2008, in The Solar System Beyond Neptune, ed. M. A. Barucci et al. (Tucson: University of Arizona Press), 161
Stier, M. T., Traub, W. A., Fazio, G. G., Wright, E. L., & Low, F. J. 1978, ApJ, 226, 347
Sykes, M. V., Cutri, R. M., Fowler, J. W., Tholen, D. J., Skrutskie, M. F., Price, S., & Tedesco, E. F. 2000, Icarus, 146, 161
Tedesco, E. F., Cellino, A., & Zappalá, V. 2005, AJ, 129, 2869
Tedesco, E. F., & Desert, F.-X. 2002, AJ, 123, 2070
Tedesco, E. F., Egan, M. P., & Price, S. D. 2002b, AJ, 124, 583
Tedesco, E. F., & Gradie, J. 1987, AJ, 93, 738
Tedesco, E. F., Noah, P. V., Noah, M., & Price, S. D. 2002a, AJ, 123, 1056
Tholen, D. J. 1984, PhD thesis, Arizona University
Thomas, N., et al. 2000, ApJ, 534, 446
Thomas, P. C., Parker, J. Wm., McFadden, L. A., Russell, C. T., Stern, S. A., Sykes, M. V., & Young, E. F. 2005, Nature, 437, 224
Trilling, D. E., et al. 2008, ApJ, 683, L199
Trilling, D. E., et al. 2010, AJ, 140, 770
Trilling, D. E., Rivkin, A. S., Stansberry, J. A., Spahr, T. B., Crudo, R. A., & Davies, J. K. 2007, Icarus, 192, 442
Veeder, G. J., Hanner, M. S., Matson, D. L., Tedesco, E. F., Lebofsky, L. A., & Tokunaga, A. T. 1989, AJ, 97, 1211
Vilas, F., Tholen, D. J., Lebofsky, L. A., Campins, H., Veeder, G. J., Binzel, R. P., & Tokunaga, A. T. 1985, Icarus, 63, 201
Warner, B. D., Harris, A. W., & Pravec, P. 2009, Icarus, 202, 134
Wolters, S. D., Green, S. F., McBride, N., & Davies, J. K. 2005, Icarus, 175, 92
Wolters, S. D., Green, S. F., McBride, N., & Davies, J. K. 2008, Icarus, 193, 535
Xu, S., Binzel, R. P., Burbine, T. H., & Bus, S. J. 1995, Icarus, 115, 1

Yang, B., Zhu, J., Gao, J., Ma, J., Zhou, X., Wu, H., & Guan, M. 2003, AJ, 126, 1086
Yoshida, F., & Nakamura, T. 2007, Planet. Space Sci., 55, 1113
Zappalà, V., Bendjoya, Ph., Cellino, A., Di Martino, M., Doressoundiram, A., Manara, A., & Migliorini, F. 2000, Icarus, 145, 4